



## Spatiotemporal dynamics of a reaction-diffusion model of pollen tube tip growth

Chenwei Tian<sup>1</sup> · Qingyan Shi<sup>2,3</sup> · Xinping Cui<sup>1</sup> · Jingzhe Guo<sup>4</sup> · Zhenbiao Yang<sup>4</sup> · Junping Shi<sup>2</sup> 

Received: 21 July 2018 / Revised: 6 June 2019 / Published online: 6 July 2019  
© Springer-Verlag GmbH Germany, part of Springer Nature 2019

### Abstract

A reaction-diffusion model is proposed to describe the mechanisms underlying the spatial distributions of ROP1 and calcium on the pollen tube tip. The model assumes that the plasma membrane ROP1 activates itself through positive feedback loop, while the cytosolic calcium ions inhibit ROP1 via a negative feedback loop. Furthermore it is proposed that lateral movement of molecules on the plasma membrane are depicted by diffusion. It is shown that bistable or oscillatory dynamics could exist even in the non-spatial model, and stationary and oscillatory spatiotemporal patterns are found in the full spatial model which resemble the experimental data of pollen tube tip growth.

**Keywords** Pollen tube tip growth · Reaction-diffusion model · Oscillation · Spatiotemporal patterns

**Mathematics Subject Classification** 92C15 · 92C80 · 35K57 · 35B36 · 35B32

---

XP Cui is partially supported by National Science Foundation Grant ATD-1222718 and the University of California, Riverside AES-CE RSAP A01869; ZB Yang is partially supported by National Institute of General Medical Sciences Grant GM100130; JP Shi is partially supported by National Science Foundation Grant DMS-1715651; QY Shi is partially supported by China Scholarship Council.

---

✉ Junping Shi  
jxshix@wm.edu

<sup>1</sup> Department of Statistics, University of California, Riverside, CA 92521, USA

<sup>2</sup> Department of Mathematics, College of William and Mary, Williamsburg, VA 23187-8795, USA

<sup>3</sup> School of Mathematical Sciences, Tongji University, Shanghai 200092, China

<sup>4</sup> Department of Botany and Plant Sciences, Center for Plant Cell Biology, University of California, Riverside, CA 92521, USA

## 1 Introduction

Cell polarity is a fundamental feature of almost all cells. It is required for the differentiation of new cells, the formation of cell shapes, and cell migration, etc (Edelstein-Keshet et al. 2013; Mogilner et al. 2012). Polar tip growth is a specialized form of cell growth, in which growth is limited to the single end of the cell, allowing the cell to rapidly elongate and penetrate tissues. Pollen tubes provide an excellent model for studying tip growth and spatiotemporal oscillation, such as  $Ca^{2+}$  oscillation (Feijó et al. 2001). As the male structure carrying sperm cells, pollen tubes protrude from pollen grains, and elongate by extremely polarized cell growth known as tip growth. They pass through several female tissues to reach the ovule, in which the sperm cells are released from the pollen tube and fuse with the egg cell and the central cell to grow an embryo and endosperm. To efficiently target to the ovule, pollen tubes grow extraordinarily fast in an oscillatory fashion which is controlled by the Rho GTPase (ROP1) molecular switch (Li et al. 1999; Yang 2008). Within the signaling network regulating polarized exocytosis to the tip of pollen tube, plasma membrane localized ROP1 at the pollen tube apex is regulated by positive and negative feedback loops through exocytosis. Polarized exocytosis regulated by active ROP1 couple with ROP1 signaling to the composition and mechanics of the cell wall (Luo et al. 2017). The resulting asymmetric cell wall structure determines the strain rates and thereby the geometry of the cell wall. To promote polar exocytosis, the ROP1 signaling network is localized dynamically to the tip plasma membrane as an apical cap, whose shape changes in an oscillatory manner as growth oscillation. Therefore, modeling the oscillatory dynamic of ROP1 distribution on the plasma membrane is the key to understand the tip growth of pollen tube.

As a key regulator of the self-organizing pollen tube system, the activity and distribution of ROP1 are fine-tuned by both positive and negative feedback mechanisms as well as slow diffusion. It has been indicated that the  $Ca^{2+}$  is involved in the negative feedback regulation of ROP1. In addition, it also has been shown that ROP1 promotes the formation of the intracellular  $Ca^{2+}$  gradients probably via the influx of extracellular  $Ca^{2+}$  (Gu et al. 2005; Li et al. 1999). In recent work (Luo et al. 2017; Xiao et al. 2016), the Yang and Cui group demonstrated that spatial distribution of active ROP1 as an apical cap can be achieved through both positive and negative feedbacks, and a gradient of guidance signal can promote ROP1 activation and lead to an asymmetric distribution of active ROP1 and result in the change of growth direction. All of these prior findings provide us the basis to uncover the quantitative principles behind the formation and regulation of rapid spatiotemporal oscillation of ROP1- $Ca^{2+}$  signaling network and their linkage to growth redirection. In this paper, we propose a reaction-diffusion model of ROP1 and  $Ca^{2+}$  distributions on the cell plasma membrane to show how ROP1 and  $Ca^{2+}$  are spatiotemporally intertwined and what are the quantitative relationship between them in order to generate the ROP1- $Ca^{2+}$  spatiotemporal oscillation.

A PDE model for yeast cell polarization was proposed in Altschuler et al. (2008) but it only considered the positive feedback. The reaction-diffusion pattern formation theory suggests that positive feedback alone cannot generate stable spatial patterns. Reaction-diffusion models for yeast cell polarization induced by pheromone spatial gradient have been established by Chou et al. (2008), Lo et al. (2014), Moore et al. (2008), Yi et al. (2007) and Zheng et al. (2011), see also (Goryachev and Pokhilko

2008; Holmes and Edelstein-Keshet 2016; Jilkin et al. 2007; Mori et al. 2011; Rätz and Röger 2012). In the recent work (Xiao et al. 2016), a PDE model for the ROP1 dynamics for the pollen tube tip growth was proposed:

$$\begin{cases} R_t = k_{pf} R^\alpha \left( R_{tot} - \int_{-L}^L R(s, \cdot) ds \right) - k_{nf} R + D_R R_{ss}, & (s, t) \in (-L, L) \times [0, T], \\ R_s(-L, t) = R_s(L, t) = 0, & t \in [0, T]. \end{cases} \quad (1.1)$$

It is shown by Xiao et al. (2016) that the positive steady state of (1.1) is unique and has a soliton-like profile which resembles the *Arabidopsis* PT experimental ROP1 data obtained in Yang lab. Moreover the parameters  $k_{pf}$  and  $k_{nf}$  were estimated based on the numerically integrated steady state profile of (1.1) and the experimental data using a constrained Least Squares (CNLS) method. The experimental data fits with the numerical steady state of (1.1) reasonably well. However the positive steady state of (1.1) indeed is unstable with respect to the time-evolution dynamics of (1.1), which suggests that some other feedback mechanism or other key activator/inhibitor in the system is not identified in (1.1). Also the model (1.1) cannot produce time-periodic patterns which occurs in the pollen tube growth.

Reaction-diffusion systems have been widely used in developmental biology modeling since the pioneer work of Turing (1952), see for example Gierer and Meinhardt (1972), Kondo and Miura (2010) and Maini et al. (1997). Rigorous bifurcation analysis for a wide range of reaction-diffusion models has been done in recent years (Chen et al. 2014; Jin et al. 2013; Wang et al. 2011, 2016; Yi et al. 2009; Zhou and Shi 2015), and the generation of spatially non-homogeneous time-periodic patterns in reaction-diffusion models with time delay has been considered by Busenberg and Huang (1996), Chen et al. (2013, 2018), Chen and Yu (2016a, b), Chen and Shi (2012), Guo (2015), Seirin Lee et al. (2011), Shi et al. (2017, 2019b), Su et al. (2009), Yan and Li (2010) and Yi et al. (2017).

Our proposed model in this paper couples the spatial  $Ca^{2+}$  dynamics with the ROP1 dynamics in (1.1). It is based on the ROP1 dynamics described in (1.1), but adds the associated  $Ca^{2+}$  dynamics which forms a reaction-diffusion model with an activator-inhibitor pair, nonlocal and time-delay effect (see Sect. 2). The baseline kinetic model is a system of two ordinary differential equations with intriguing dynamics: (i) bistability; (ii) limit cycles generated through Hopf bifurcations; (iii) degenerate trivial steady state (0, 0). A detailed analysis and classification is given for the kinetic system in Sect. 3. In Sect. 4, the analysis and simulation of the reaction-diffusion system is given. It is demonstrated that a rich spectrum of spatiotemporal patterns can be produced by our proposed model: non-constant steady states, spatially homogeneous time-periodic solutions, and various spatially nonhomogeneous time-periodic solutions. Of particular interest to the pollen tube tip growth is the spatially nonhomogeneous time-periodic solutions, which predicts the ROP1- $Ca^{2+}$  spatiotemporal oscillation. Indeed our numerical finding in certain parameter range qualitatively matches with experimental data generated in Yang Lab (Hwang et al. 2005), which partially validates the proposed reaction-diffusion model and underlying modeling principle. Some concluding remarks are given in Sect. 5.

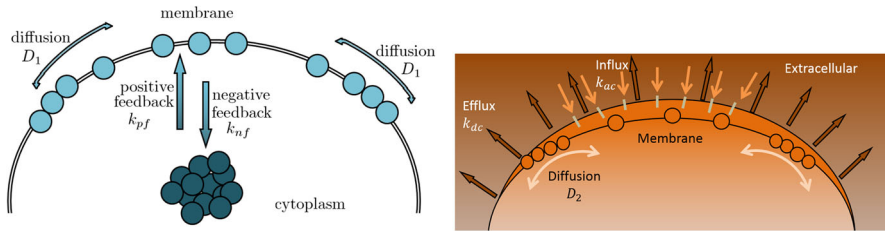


**Fig. 1** ROP1 and  $Ca^{2+}$  polarization dynamics. Left: ROP1 dynamics; Right:  $Ca^{2+}$  dynamics

## 2 Model

To model the cell-signaling process on the membrane, we simplify the cell membrane as a one-dimensional spatial domain  $x \in (-L, L)$ , where  $x$  is the (signed) distance from the tip of the membrane  $x = 0$ . Note that for simplicity, we ignore the geometric curvature of the membrane in the current model. The main variables in the models are the active ROP1 concentration  $R(x, t)$  and the Calcium ion  $Ca^{2+}$  concentration at the location  $x$  and time  $t$ . Moreover, we set  $L$  to be large enough so that the ROP1 and  $Ca^{2+}$  concentration gradients are close to zero on the boundary, so we assume that  $R$  and  $C$  satisfy no-flux boundary condition:

$$\frac{\partial R(x, t)}{\partial x} = \frac{\partial C(x, t)}{\partial x} = 0, \quad x = -L, L. \quad (2.1)$$

The redistribution of signaling molecules ROP1 is determined by the rates of four fundamental transport mechanisms (Altschuler et al. 2008): (1) recruitment ( $k_{fb}$ ) of cytoplasmic molecules to the locations of membrane-bound signaling molecules; (2) spontaneous association ( $k_{on}$ ) of cytoplasmic molecules to random locations on the plasma membrane; (3) lateral diffusion ( $D$ ) of molecules along the membrane; and (4) random disassociation ( $k_{off}$ ) of signaling molecules from the membrane.

In our model, we eliminate the spontaneous term because the spontaneous rate  $k_{on}$  is much smaller than  $k_{fb}$  and  $k_{off}$ . Altschuler et al. (2008) proposed a stochastic model showing that no cluster will be formed if  $k_{on}$  is not small, and then most particles will arrive on the membrane through spontaneous associations rather than recruitment. So we can assume that  $k_{on}$  is small enough. Moreover, the time between two spontaneous event follows an exponential distribution with expectation  $T_{on} = (k_{on}(1 - h_{eq})N)^{-1}$ . When  $k_{on}$  is small,  $T_{on}$  will be large which leads to a long time between two spontaneous events. Our partial differential equation model describes the change of distribution of ROP1 intensity in a short period of time. Therefore, we eliminate the spontaneous term when we model the cell-signaling process.

In this case, the ROP1 polarization dynamics without spontaneous association can be simplified as three main procedures (see Fig. 1 left panel): (1) activation of inactive ROP1; (2) inhibition of active ROP1; (3) lateral diffusion of molecules along the membrane. The activation of ROP1 can be considered as a positive feedback while the deactivation of ROP1 as a negative feedback. Both activation and inhibition rates are proportional to substrate concentrations.

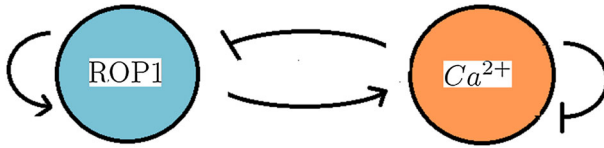


Fig. 2 Interaction diagram of ROP1 and  $Ca^{2+}$

The lateral movement of ROP1 is modeled by a diffusion term  $D_1 \frac{\partial^2 R(x, t)}{\partial x^2}$ , where  $D_1$  is the diffusion coefficient of ROP1. As for activation of ROP1, it is shown by biology model simulation, the activation rate is proportional to  $R^\alpha$  where the exponent satisfies  $1 < \alpha < 2$ . Moreover, since majority of inactive ROP1 are in cytoplasm with high mobility, the activation rate is proportional to the total amount of cytoplasmic molecules (i.e.  $R_{total} - \int_{-L}^L R(x, t) dx$ ) with rate  $k_{pf}$ . On the other hand, most active ROP1 are on the membrane. Since molecules on the membrane have much less mobility, the inhibition rate is proportional to the density of molecules (i.e.  $R(x, t)$ ) at any given location with rate  $k_{nf}$ . Moreover,  $Ca^{2+}$  can inhibit ROP1 with some threshold  $k_h$  and an inhibition function

$$g(C) = \frac{C^2}{C^2 + k_h^2}. \tag{2.2}$$

Here  $g(C)$  is a Hill function which shows a transition from low inhibition rate at low Calcium density, and a high but bounded inhibition rate at a high Calcium density. The constant  $k_h$  is the half-saturation value indicating the threshold between the low and high Calcium density. Hence  $R(x, t)$  satisfies a reaction-diffusion equation with a nonlocal integral term:

$$\begin{aligned} \frac{\partial R(x, t)}{\partial t} = & k_{pf} R^\alpha(x, t) \left( R_{total} - \int_{-L}^L R(x, t) dx \right) \\ & - k_{nf} R(x, t) g(C(x, t)) + D_1 \frac{\partial^2 R(x, t)}{\partial x^2}. \end{aligned} \tag{2.3}$$

On the other hand, we simplify the  $Ca^{2+}$  activities as following three procedures: (1) influx of  $Ca^{2+}$ ; (2) self-decay of  $Ca^{2+}$ ; and (3) diffusion of  $Ca^{2+}$  along the membrane (see Fig. 1 right panel). The diffusion of  $Ca^{2+}$  is given by  $D_2 \frac{\partial^2 C(x, t)}{\partial x^2}$ , where  $D_2$  is the diffusion coefficient of  $Ca^{2+}$ . The  $Ca^{2+}$  ions could flow into the cell through Calcium channel on the membrane, and the  $Ca^{2+}$  inflow is controlled by ROP1 with rate  $k_{ac}$ . Also there is a time delay  $\tau$  in this promotion. In this work, we model  $Ca^{2+}$  promotion with  $k_{ac} R(x, t - \tau)$  to show a linear response of Calcium influx to the ROP1 density, which is supported by several studies from Yang lab (Hwang et al. 2005; Li et al. 1999; Yan et al. 2009). On the other hand, self-decay of  $Ca^{2+}$  is proportional to substrate concentration at a certain rate  $k_{dc}$ . Therefore, the

$Ca^{2+}$  activities are described by a reaction-diffusion equation with time-delay:

$$\frac{\partial C(x, t)}{\partial t} = k_{ac}R(x, t - \tau) - k_{dc}C(x, t) + D_2 \frac{\partial^2 C(x, t)}{\partial x^2}. \quad (2.4)$$

Note that ROP1 activates both ROP1 and  $Ca^{2+}$  growth, and  $Ca^{2+}$  inhibits both ROP1 and  $Ca^{2+}$  (see Fig. 2).

Now summarizing the above description, adding the proper initial conditions, we have the following full system for the interaction between the ROP1 and  $Ca^{2+}$  on the cell membrane:

$$\begin{cases} R_t = k_{pf}R^\alpha \left( R_{total} - \int_{-L}^L R dx \right) - k_{nf} \frac{RC^2}{C^2 + k_h^2} + D_1 R_{xx}, & (x, t) \in (-L, L) \times (0, T), \\ C_t = k_{ac}R(x, t - \tau) - k_{dc}C + D_2 C_{xx}, & (x, t) \in (-L, L) \times (0, T), \\ R_x(x, t) = C_x(x, t) = 0, & x = -L, L, \\ R(x, t) = R_0(x, t), & (x, t) \in (-L, L) \times [-\tau, 0], \\ C(x, 0) = C_0(x), & x \in (-L, L). \end{cases} \quad (2.5)$$

Here  $R_t$ ,  $C_t$ ,  $R_{xx}$ ,  $C_{xx}$  are abbreviated notations for partial derivatives, and  $R = R(x, t)$ ,  $C = C(x, t)$  except the term with time delay.

To reduce the number of parameters in the problem and convert the equation into a dimensionless form, we introduce the normalized quantities:

$$\begin{aligned} \tilde{t} &= k_{dc}t, \quad \tilde{x} = \sqrt{\frac{k_{dc}}{D_2}}x, \quad \tilde{R} = \frac{2LR}{R_{total}}, \quad \tilde{C} = \frac{2Lk_{dc}C}{R_{total}k_{ac}}, \quad (2.6) \\ k_1 &= \frac{2Lk_{pf}}{k_{dc}} \left( \frac{R_{total}}{2L} \right)^\alpha, \quad k_2 = \frac{k_{nf}}{2Lk_{pf}} \left( \frac{2L}{R_{total}} \right)^\alpha, \quad k_3 = \frac{2Lk_h k_{dc}}{k_{ac}R_{total}}, \quad D = \frac{D_1}{D_2}, \quad (2.7) \end{aligned}$$

$$\tilde{\tau} = k_{dc}\tau, \quad \tilde{L} = L\sqrt{\frac{k_{dc}}{D_2}}, \quad \tilde{T} = k_{dc}T. \quad (2.8)$$

With these normalized quantities, the PDE model (2.5) is rewritten in the following normalized form:

$$\begin{cases} \tilde{R}_{\tilde{t}} = k_1 \tilde{R}^\alpha \left( 1 - \frac{1}{2\tilde{L}} \int_{-\tilde{L}}^{\tilde{L}} \tilde{R} d\tilde{x} \right) - k_1 k_2 \frac{\tilde{R}\tilde{C}^2}{\tilde{C}^2 + k_3^2} + D \tilde{R}_{\tilde{x}\tilde{x}}, & (\tilde{x}, \tilde{t}) \in (-\tilde{L}, \tilde{L}) \times (0, \tilde{T}), \\ \tilde{C}_{\tilde{t}} = \tilde{R}(\tilde{x}, \tilde{t} - \tilde{\tau}) - \tilde{C} + \tilde{C}_{\tilde{x}\tilde{x}}, & (\tilde{x}, \tilde{t}) \in (-\tilde{L}, \tilde{L}) \times (0, \tilde{T}), \\ \tilde{R}_{\tilde{x}}(\tilde{x}, \tilde{t}) = \tilde{C}_{\tilde{x}}(\tilde{x}, \tilde{t}) = 0, & \tilde{x} = -\tilde{L}, \tilde{L}, \\ \tilde{R}(\tilde{x}, \tilde{t}) = \tilde{R}_0(\tilde{x}, \tilde{t}), & (\tilde{x}, \tilde{t}) \in (-\tilde{L}, \tilde{L}) \times [-\tilde{\tau}, 0], \\ \tilde{C}(\tilde{x}, 0) = \tilde{C}_0(\tilde{x}), & \tilde{x} \in (-\tilde{L}, \tilde{L}). \end{cases} \quad (2.9)$$

Dropping the  $\sim$  in (2.9), we have the system

$$\begin{cases} R_t = k_1 R^\alpha \left( 1 - \frac{1}{2L} \int_{-L}^L R dx \right) - k_1 k_2 \frac{RC^2}{C^2 + k_3^2} + DR_{xx}, & (x, t) \in (-L, L) \times (0, T), \\ C_t = R(x, t - \tau) - C + C_{xx}, & (x, t) \in (-L, L) \times (0, T), \\ R_x(x, t) = C_x(x, t) = 0, & x = -L, L, \\ R(x, t) = R_0(x, t), & (x, t) \in (-L, L) \times [-\tau, 0], \\ C(x, 0) = C_0(x), & x \in (-L, L). \end{cases} \tag{2.10}$$

From now on, we will analyze the dynamics behavior of the simplified system (2.10). Indeed, in this paper, we will only consider the case that  $\tau = 0$  to show the rich dynamics of corresponding ODE and PDE models, and the effect of delay will be considered in a future work.

### 3 Non-spatial dynamics

In system (2.10), if the initial conditions  $(R_0(x, t), C_0(x))$  are spatially homogeneous and  $\tau = 0$ , then the corresponding solution of (2.10) is also spatially homogeneous and it satisfies

$$\begin{cases} R_t = k_1 R^\alpha (1 - R) - k_1 k_2 \frac{RC^2}{C^2 + k_3^2}, \\ C_t = R - C. \end{cases} \tag{3.1}$$

The steady states of (3.1) satisfy

$$\begin{cases} k_1 R^\alpha (1 - R) - k_1 k_2 \frac{RC^2}{C^2 + k_3^2} = 0, \\ R - C = 0. \end{cases} \tag{3.2}$$

A nonnegative steady state is either the trivial one  $(R, C) = (0, 0)$ , or a positive one satisfying

$$R^{\alpha-1} (1 - R) - k_2 \frac{C^2}{C^2 + k_3^2} = 0, \quad C = R. \tag{3.3}$$

Then (3.3) is equivalent to  $C = R$  and

$$f(R) \equiv k_2 - R^{\alpha-3} (1 - R) (R^2 + k_3^2) = 0. \tag{3.4}$$

The following result shows the existence and exact multiplicity of roots  $R$  of (3.4), which also reveals the existence and exact multiplicity of steady states of (3.1) in form  $(R, R)$ .

**Proposition 3.1** *There exists a constant  $k_{31} > 0$  such that*

1. *If  $0 < k_3 < k_{31}$ , then there exists  $0 < k_{21} < k_{22}$  which depend on  $k_3$  and  $\alpha$  such that*

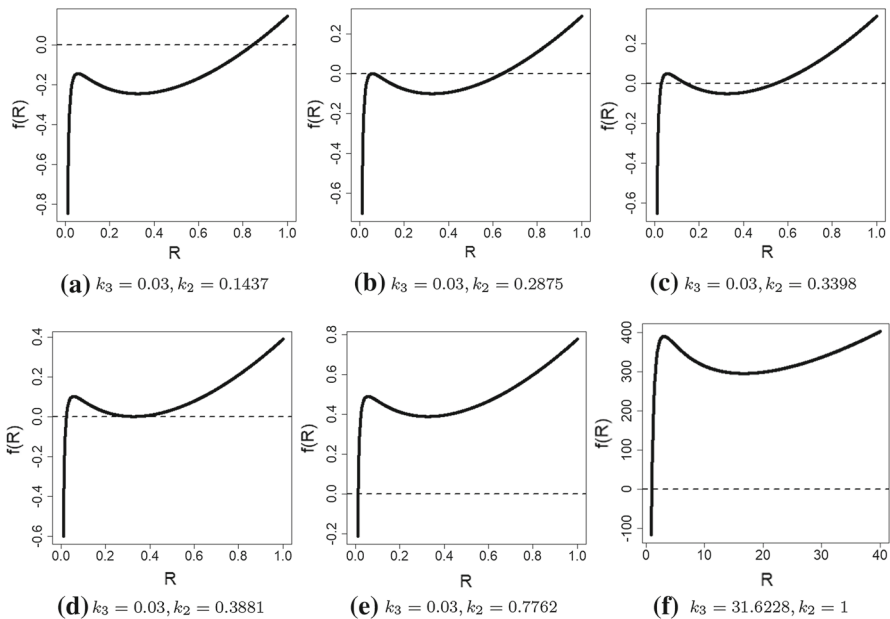


**Fig. 3** Graphs of  $f(R)$  with  $\alpha = 1.5$  and varying  $(k_2, k_3)$

- (a) when  $0 < k_2 < k_{21}$ , there is a unique positive root  $R_3$  for (3.4) (see Fig. 3a);  
 (b) when  $k_2 > k_{22}$ , there is a unique positive root  $R_1$  for (3.4) (see Fig. 3e);  
 (c) when  $k_2 = k_{21}$  or  $k_2 = k_{22}$ , then there are exactly two positive roots  $R_1, R_3$  satisfying  $R_1 < R_3$  for (3.4) (see Fig. 3b, d);  
 (d) when  $k_{21} < k_2 < k_{22}$ , there are exactly three positive roots  $R_1, R_2, R_3$  satisfying  $R_1 < R_2 < R_3$  for (3.4) (see Fig. 3c).

2. If  $k_3 > k_{31}$ , then for any  $k_2 > 0$ , there is a unique positive root  $R_1$  for (3.4) (see Fig. 3f).

The proof of Proposition 3.1 is given in Appendix. From Proposition 3.1, (3.1) possesses one, or two, or three positive steady states depending on the parameter values of  $k_2$  and  $k_3$ . We denote the positive steady states of (3.1) by  $(R_j, C_j) = (R_j, R_j)$  ( $1 \leq j \leq 3$ ), where  $R_j$  is the root of (3.4) as shown in Proposition 3.1, and  $C_j = R_j$ . Figure 4 shows the regions of parameters  $(k_2, k_3)$  where (3.1) has 1 or 3 positive steady states. When  $k_3 > k_{31}$ , the bifurcation diagram in  $(k_2, R, C)$ -space is a monotone curve (see Fig. 5b, c), while when  $0 < k_3 < k_{31}$ , the corresponding bifurcation diagram is an S-shaped one with two saddle-node bifurcation points at  $k_2 = k_{21}$  and  $k_2 = k_{22}$  (see Fig. 5a). When the parameter  $k_2$  varies, the bifurcation diagram depicts a typical hysteresis scenario with a bistable structure. Similar bifurcation structure have been found in various biological models of spruce budworm population (Ludwig et al. 1978), shallow lakes (Scheffer et al. 2001, 1993), coral reef (Li et al. 2014; Mumby et al. 2007), and forest and savanna (Ding et al. 2017; Staver et al. 2011a, b).

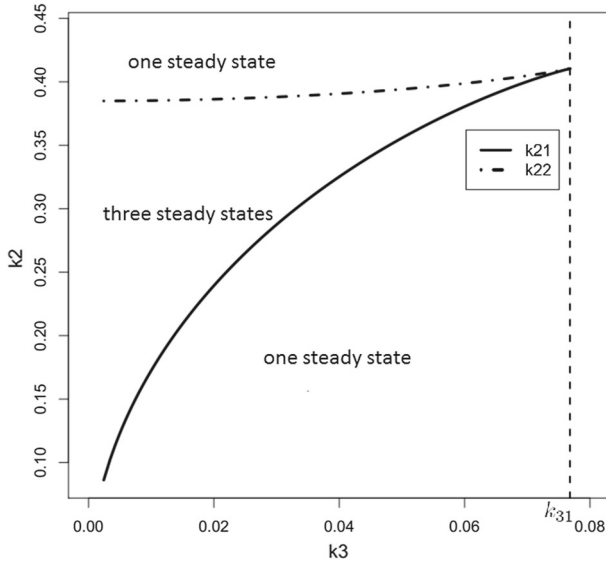


**Fig. 4** The number of positive steady states of system (3.1) for different values of  $(k_2, k_3)$  with  $\alpha = 1.5$ . Here the horizontal axis is  $k_3$  and vertical axis is  $k_2$

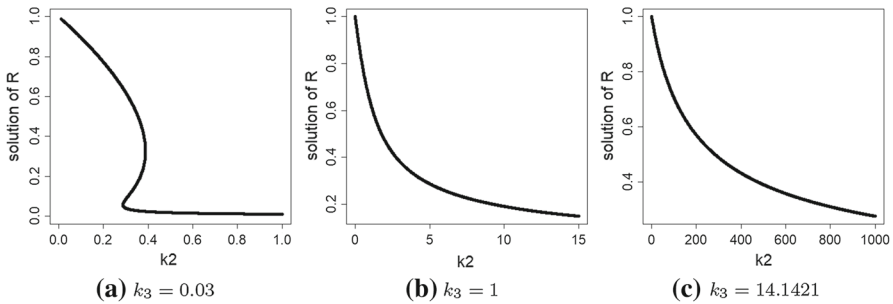


**Fig. 5** Bifurcation diagrams of system (3.1) with  $\alpha = 1.5$

Next we consider the local stability of the steady states  $(0, 0)$  and  $(R_j, R_j)$  ( $1 \leq j \leq 3$ ) with respect to (3.1). First at steady state  $(0, 0)$ , the Jacobian matrix is  $\begin{pmatrix} 0 & 0 \\ 1 & -1 \end{pmatrix}$ . Therefore we have two eigenvalues  $\lambda_1 = 0$  and  $\lambda_2 = -1 < 0$  which indicates that  $(0, 0)$  is a degenerate steady state. One can apply the theory of two-dimensional dynamical system to obtain the following description of the dynamics of (3.1) near  $(0, 0)$ :

**Proposition 3.2** For any  $k_1, k_2, k_3 > 0$ , there exists a  $\delta > 0$  such that in the neighborhood  $B = \{(R, C) : 0 < R < \delta, 0 < C < \delta\}$  of  $(0, 0)$ ,

- (3.1) has a unique center manifold  $W^c = \{(R, h_c(R)) : 0 \leq R < \delta\}$  for (3.1) such that  $h_c(0) = 0$  and  $h'_c(0) = 1$ , and the orbit of (3.1) on  $W_c$  is unstable;

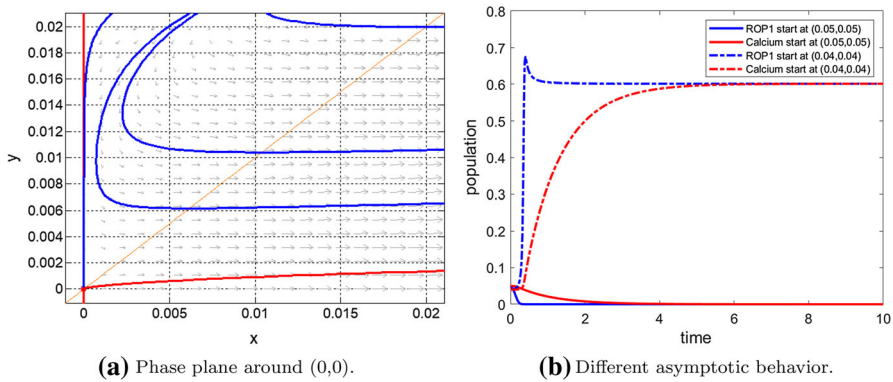


**Fig. 6** Dynamical behavior of (3.1) near (0, 0). Here  $\alpha = 1.5, k_1 = 175, k_2 = 0.31, k_3 = 0.0316$ , and the initial conditions for the solution orbits in the right panel are  $(R(0), C(0)) = (0.05, 0.05)$  and  $(0.04, 0.04)$

2. there exists a function  $h_s : (0, \delta) \rightarrow (0, \delta)$  such that the region  $O = \{(R, C) : 0 \leq R \leq h_s(C), 0 < C < \delta\}$  is invariant, and for any  $(R_0, C_0) \in O$ , the solution  $(R(t), C(t))$  of (3.1) with  $(R(0), C(0)) = (R_0, C_0)$  satisfies  $\lim_{t \rightarrow \infty} (R(t), C(t)) = (0, 0)$ .
3. other orbits in  $B$  exhibit saddle behavior near  $(0, 0)$ , that is, the orbit does not approach  $(0, 0)$  as  $t \rightarrow \infty$  or  $t \rightarrow -\infty$ , and for  $t > T$ , the orbit leaves the neighborhood  $B$ .

The proof of Proposition 3.2 is given in Appendix. It shows that there is a “horn”-shaped region belonging to the basin of attraction of the origin  $(0, 0)$ . Indeed for any parameter values, if the initial value of  $Ca^{2+}$   $C_0$  is sufficiently large, then the solution will converge to  $(0, 0)$  (see Fig. 6). So our subsequent discussion will be for the remaining part of the phase portrait in which the orbits do not converge to  $(0, 0)$ .

For positive steady states, we linearize (3.1) at a steady state  $(R_j, R_j)$  ( $j = 1, 2, 3$ ), then we obtain the Jacobian matrix as

$$J(R_j, R_j) = \begin{pmatrix} k_1 R_j f'_1(R_j) & -k_1 R_j f'_2(R_j) \\ 1 & -1 \end{pmatrix}, \tag{3.5}$$

where

$$f_1(R) = R^{\alpha-1}(1 - R), \quad f_2(R) = \frac{k_2 R^2}{R^2 + k_3^2}. \tag{3.6}$$

Hence we find that

$$\text{Tr}(J(R_j, R_j)) = k_1 R_j f'_1(R_j) - 1, \tag{3.7}$$

$$\text{Det}(J(R_j, R_j)) = k_1 R_j (f'_2(R_j) - f'_1(R_j)). \tag{3.8}$$

We recall that a steady state  $(R, R)$  of (3.1) is a sink or spiral sink if both eigenvalues of  $J(R, R)$  are of negative real parts; it is a source or spiral source if both eigenvalues of  $J(R, R)$  are of positive real parts; and it is a saddle if  $J(R, R)$  has one positive and

one negative eigenvalue. From the trace-determinant theory, it is easy to know that  $(R, R)$  is a sink or spiral sink if  $\text{Tr}(J) < 0$  and  $\text{Det}(J) > 0$ ; it is a source or spiral source if  $\text{Tr}(J) > 0$  and  $\text{Det}(J) > 0$ ; and it is a saddle if  $\text{Tr}(J) \in \mathbb{R}$  and  $\text{Det}(J) < 0$ .

For our next result regarding the local stability of the positive steady state  $(R_j, R_j)$  ( $j = 1, 2, 3$ ) obtained above, we determine the stability using the trace and determinant of  $J(R, C)$ . We also observe that the steady states of (3.1) are independent of parameter  $k_1$ , but  $k_1$  does affect the stability of steady states. For fixed  $\alpha \in (1, 2)$  and  $k_3 > 0$ , and any  $0 < R < 1$ , the pair  $(R, R)$  can be a steady state of (3.1) for exactly one value of  $k_2 > 0$  by the relation (from (3.2)):

$$k_2 = R^{\alpha-3}(1 - R)(R^2 + k_3^2). \tag{3.9}$$

That is, for fixed  $\alpha \in (1, 2)$  and  $k_3 > 0$ , the set of steady states of (3.1) can be parameterized by  $R$  as a bifurcation diagram (see Fig. 5):

$$\Sigma = \{(k_2(R), R, R) : R \in (0, 1)\}, \tag{3.10}$$

where  $k_2(R)$  is given by (3.9). Now we state our results on the local stability of the positive steady state in terms of parametrization in (3.10).

**Theorem 3.3** *Suppose that  $\alpha \in (1, 2)$  and  $k_3 > 0$ , and  $k_2(R)$  is defined as in (3.9) so that  $(R, R)$  is a positive steady state of (3.1) with  $k_2 = k_2(R)$  for  $0 < R < 1$ .*

1. *If  $k_3 > k_{31}$  (defined in Proposition 3.1), then  $\text{Det}(J(R, R)) > 0$  for any  $R \in (0, 1)$ ; and if  $0 < k_3 < k_{31}$ , then there exist  $r_1, r_2 > 0$  such that  $\text{Det}(J(R, R)) > 0$  for  $R \in (0, r_1) \cup (r_2, 1)$ , and  $\text{Det}(J(R, R)) < 0$  for  $R \in (r_1, r_2)$ . Here  $k_2(r_1) = k_{21}$  and  $k_2(r_2) = k_{22}$  (defined in Proposition 3.1).*
2. *Define*

$$k_{11} = \frac{\alpha^{2\alpha-1}}{(\alpha - 1)^{2\alpha-1}}. \tag{3.11}$$

*If  $0 < k_1 < k_{11}$ , then  $\text{Tr}(J(R, R)) < 0$  for any  $R \in (0, 1)$ ; and if  $k_1 > k_{11}$ , then there exist  $0 < \tilde{R}_1 < \tilde{R}_2$  such that  $\text{Tr}(J(R, R)) < 0$  for  $R \in (0, \tilde{R}_1) \cup (\tilde{R}_2, 1)$ , and  $\text{Tr}(J(R, R)) > 0$  for  $R \in (\tilde{R}_1, \tilde{R}_2)$ .*

According to Theorem 3.3, we can have following results for  $0 < k_3 < k_{31}$ , when there are at least one and at most three positive steady state of (3.1):

1. The middle positive steady state  $(R_2, R_2)$  is always a saddle.
2. The largest positive steady state  $(R_3, R_3)$  or the smallest one  $(R_1, R_1)$  is either a sink or spiral sink, or a source or spiral source, but it is not a saddle.
3. Define

$$I_s = ((0, r_1) \cup (r_2, 1)) \cap ((0, \tilde{R}_1) \cup (\tilde{R}_2, 1)). \tag{3.12}$$

Then when  $R \in I_s$ , the positive steady state  $(R, R)$  is a sink or spiral sink which is locally asymptotically stable. In particular, when  $R > 0$  is sufficiently small or when  $R$  is close to 1, then  $(R, R)$  is a sink or spiral sink.

## 4. Define

$$I_u = ((0, r_1) \cup (r_2, 1)) \cap (\tilde{R}_1, \tilde{R}_2). \quad (3.13)$$

Then when  $R \in I_u$ , the positive steady state  $(R, R)$  is a source or spiral source which is unstable.

The proof of Theorem 3.3 is in the Appendix. Note that the stable regime  $I_s$  is always not an empty set as it contains a right neighborhood of  $R = 0$  and a left neighborhood of  $R = 1$ , but  $I_s$  may also contain another connected component which is disconnected from  $R = 0$  and  $R = 1$ . The unstable regime  $I_u$  could be empty, and that happens when  $0 < k_1 < k_{11}$ . However  $I_u$  is not empty when  $k_1$  is chosen as sufficiently large. Indeed for fixed  $k_3 > 0$ , one has that

$$\lim_{k_1 \rightarrow \infty} \tilde{R}_1 = 0, \quad \lim_{k_1 \rightarrow \infty} \tilde{R}_2 = \frac{\alpha - 1}{\alpha}. \quad (3.14)$$

The local stability analysis given in Theorem 3.3 can be used to guide our classification of global dynamics of (3.1). A complete classification in terms of parameters  $(k_1, k_2, k_3)$  is rather exhaustive and it will not be given here. Here we focus on in which cases, the system (3.1) shows sustained temporal oscillations. The follow result classifies the occurrence of Hopf bifurcations in terms of parameters  $k_1, k_2$  and  $k_3$ .

**Proposition 3.4** *Suppose that  $\alpha \in (1, 2)$ , and define*

$$g(R) = R^{\alpha-1}[(\alpha - 1) - \alpha R]. \quad (3.15)$$

Let  $k_{31}, k_{11}$  be defined as in Proposition 3.1 and (3.11) respectively, and let  $r_1, r_2, \tilde{R}_1, \tilde{R}_2 > 0$  be defined in Theorem 3.3. We also define  $\tilde{k}_{21} = k_2(\tilde{R}_1)$  and  $\tilde{k}_{22} = k_2(\tilde{R}_2)$ .

1. If  $k_3 > k_{31}$ , (3.1) has a unique positive steady state for all  $k_1, k_2 > 0$ . Moreover
  - (a) When  $k_1 < k_{11}$ , the unique positive steady state of (3.1) is a sink or spiral sink for any  $k_2 > 0$ . (see Fig. 7a)
  - (b) When  $k_1 > k_{11}$ , the unique positive steady state of (3.1) is a sink or spiral sink for  $k_2 \in (0, \tilde{k}_{22}) \cup (\tilde{k}_{21}, \infty)$ , and is unstable for  $k_2 \in (\tilde{k}_{22}, \tilde{k}_{21})$ ; Hopf bifurcations occur at  $k_2 = \tilde{k}_{21}$  and  $k_2 = \tilde{k}_{22}$ , and there exists at least one periodic orbit for  $k_2 \in (\tilde{k}_{22}, \tilde{k}_{21})$ . (see Fig. 7b)
2. If  $0 < k_3 < k_{31}$ , (3.1) has at least one and at most three positive steady states, and when there exist three positive steady states, the middle one  $(R_2, R_2)$  is a saddle. Moreover
  - (c) If  $k_1 > 1/g(r_2)$ , then Hopf bifurcations occur at  $\tilde{k}_{22}$  on the large steady state  $(R_3, R_3)$  and at  $\tilde{k}_{21}$  on the small steady state  $(R_1, R_1)$  of (3.1). (see Fig. 7c)
  - (d) If  $1/g(r_1) < k_1 < 1/g(r_2)$ , then the large positive steady state  $(R_3, R_3)$  is always a sink or spiral sink, and a Hopf bifurcation occurs at  $\tilde{k}_{21}$  on the small positive steady state  $(R_1, R_1)$  of (3.1). (see Fig. 7d)

(e) Define

$$\tilde{k}_3 = \sqrt{\frac{(\alpha - 1)^5}{\alpha^3(-\alpha^2 + 5\alpha - 2)}}. \tag{3.16}$$

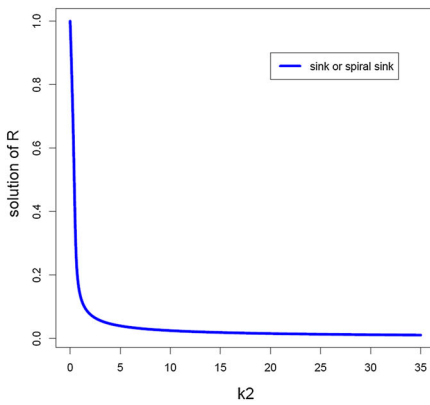
If  $0 < k_1 < 1/g(r_1)$  and  $0 < k_3 < \tilde{k}_3$ , or  $0 < k_1 < k_{11}$  and  $\tilde{k}_3 < k_3 < k_{31}$ , then both the large positive steady state  $(R_3, R_3)$  and the small positive steady state  $(R_1, R_1)$  are always sink or spiral sink, and there is no Hopf bifurcation occurring. (see Fig. 7e)

(f) If  $k_{11} < k_1 < 1/g(r_1)$  and  $\tilde{k}_3 < k_3 < k_{31}$ , then the large positive steady state  $(R_3, R_3)$  is always a sink or spiral sink, and Hopf bifurcations occur at  $\tilde{k}_{21}$  and  $\tilde{k}_{22}$  on the small positive steady state  $(R_1, R_1)$  of (3.1). (see Fig. 7f)

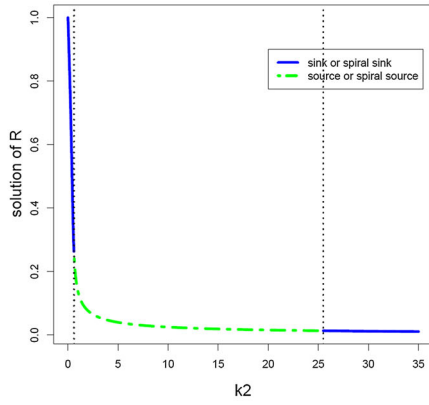
The proof of Proposition 3.4 is in the Appendix. The six bifurcation diagrams of steady states and Hopf bifurcations are shown in Fig. 7, and a classification of  $(k_3, k_1)$  parameter regions in which Hopf bifurcations with parameter  $k_2$  can occur is summarized in Fig. 8.

Guided by bifurcation diagrams above, there are following six possible dynamic phase planes and dynamics of  $(R(t), C(t))$  solutions. Note that from Proposition 3.2, there is always a region of initial conditions that orbits starting from there converge to the origin  $(0, 0)$  as  $t \rightarrow \infty$ . So in the following we only describe the dynamics below the basin of attraction of  $(0, 0)$ .

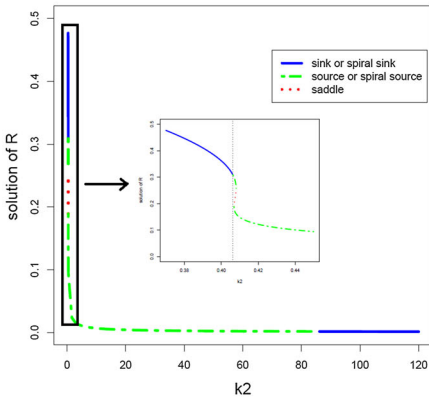
1. There is only one positive steady state  $R_1$ , which is a sink or spiral sink. All the solutions will converge to  $R_1$ . For example, when  $\alpha = 1.5, k_1 = 9.5, k_2 = 1, k_3 = 0.06$ , there is a spiral sink at  $R_1 = 0.02587$ . (See Fig. 9 upper row)
2. There is only one positive steady state  $R_1$ , which is a source or spiral source, and there is a limit cycle around  $R_1$ . For example, when  $\alpha = 1.5, k_1 = 15, k_2 = 1, k_3 = 0.06$ , there is a limit cycle around positive steady state  $R_1 = 0.02587$ . (See Fig. 9 lower row)
3. There are three positive steady states  $R_1, R_2$  and  $R_3$ ;  $R_2$  is a saddle point while  $R_1$  and  $R_3$  are sinks or spiral sinks. A solution will converge to either  $R_1$  or  $R_3$  depending on the initial value. For example, when  $\alpha = 1.5, k_1 = 5, k_2 = 0.4035, k_3 = 0.0707$ , there are two sinks  $R_1 = 0.1418$  and  $R_3 = 0.3194$ . The solution converges to  $R_1 = 0.1418$  if the initial value is  $(R(0), C(0)) = (0.1, 0.4)$ , while to  $R_3 = 0.3194$  if  $(R(0), C(0)) = (0.4, 0.1)$ . (See Fig. 10)
4. There are three positive steady states  $R_1$ , which is a source,  $R_2$ , which is a saddle point,  $R_3$ , which is a sink. Here except the stable manifold of  $R_2$ , all other solutions converge to  $R_3$ . For example, when  $\alpha = 1.5, k_1 = 12, k_2 = 0.31, k_3 = 0.0316$ , the sink  $R_3 = 0.6013$  attracts most of initial condition, and Fig. 11 shows an orbit connecting  $R_1$  to  $R_3$ . It is also possible that there is a limit cycle around  $R_1$ , but the parameter range for that case is not robust.
5. There are three positive steady states  $R_1, R_2$  and  $R_3$ .  $R_2$  is a saddle point while  $R_1$  and  $R_3$  are source or spiral source. Again the parameter range supporting such dynamics is not robust enough so we do not include a phase portrait for that case here.



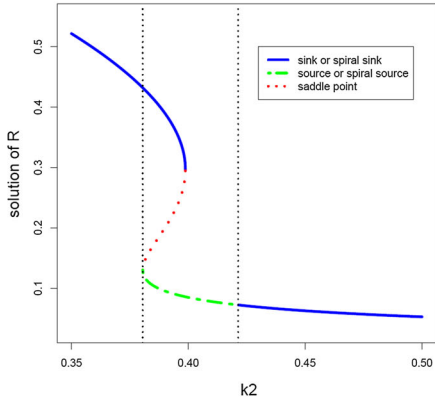
(a)  $k_3 = 0.2, k_1 = 4.5$



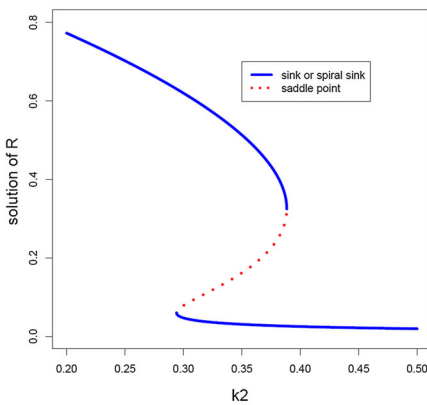
(b)  $k_3 = 0.2, k_1 = 18$



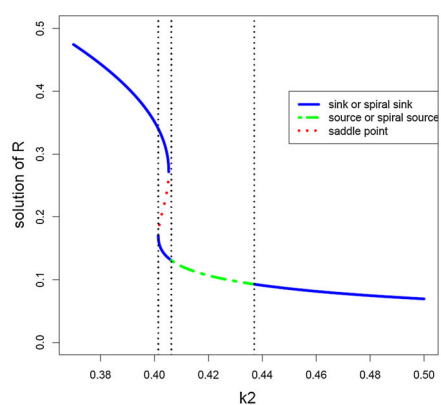
(c)  $k_3 = 0.0742, k_1 = 50$



(d)  $k_3 = 0.06, k_1 = 9.5$



(e)  $k_3 = 0.0316, k_1 = 9.5$



(f)  $k_3 = 0.0707, k_1 = 9.1$

**Fig. 7** Possible bifurcation diagrams of (3.1) with parameter  $k_2$ . Here the horizontal axis is  $k_2$  and the vertical axis is  $R$ ,  $\alpha = 1.5$  and  $k_1, k_3$  are specified for each diagram

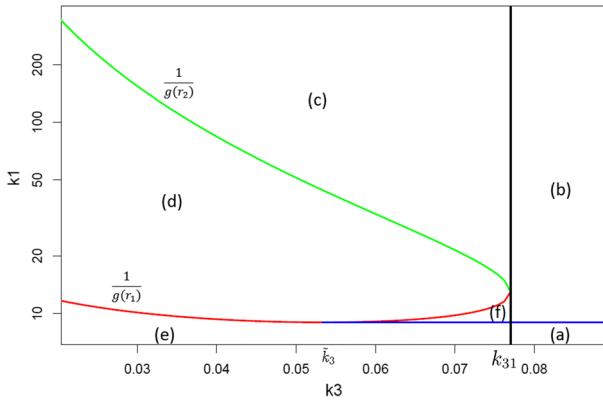


**Fig. 8** Classification of  $(k_3, k_1)$  parameter region for Hopf Bifurcation occurrence with  $\alpha = 1.5$ . Here regions (a) to (f) represent  $(k_3, k_1)$  parameter regions of cases (a) to (f) in Proposition 3.4, respectively

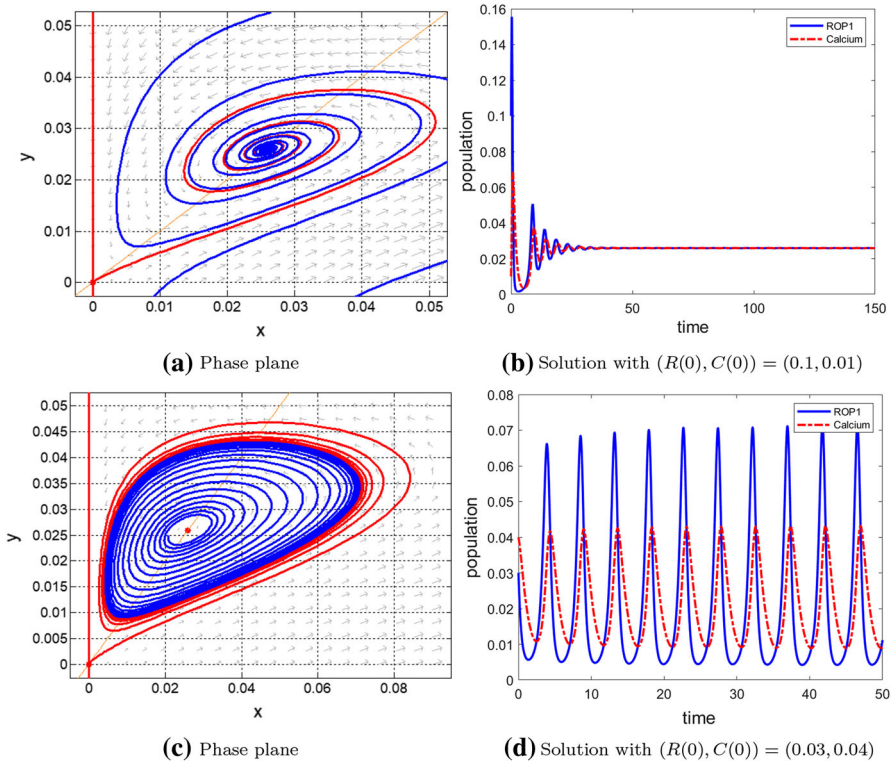


**Fig. 9** Dynamic behavior of (3.1). Here  $\alpha = 1.5, k_2 = 1, k_3 = 0.06$ ; Upper:  $k_1 = 9.5$ ; Lower:  $k_1 = 15$

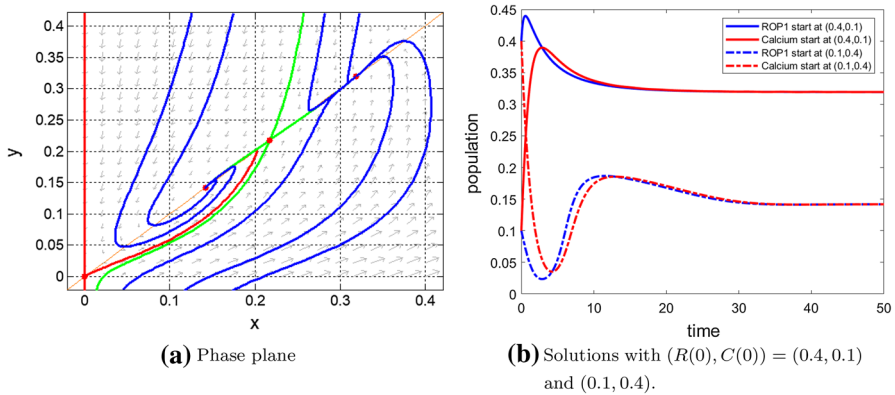


Fig. 10 Dynamic behavior of (3.1). Here  $\alpha = 1.5, k_1 = 5, k_2 = 0.4035, k_3 = 0.0707$

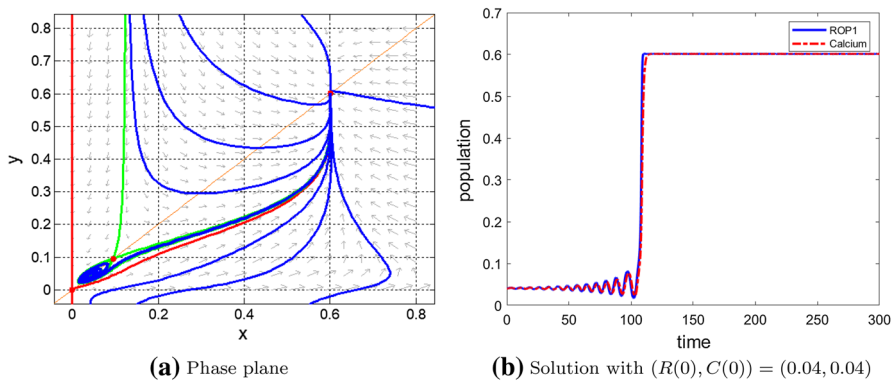


Fig. 11 Dynamic behavior of (3.1). Here  $\alpha = 1.5, k_1 = 12, k_2 = 0.31, k_3 = 0.0316$

### 4 Spatial dynamics

In this section, we consider the dynamics of the reaction-diffusion model (2.10) which is also with nonlocal term and delay. First we consider the model without the time delay:

$$\begin{cases} R_t = DR_{xx} + k_1 R^\alpha \left( 1 - \frac{1}{2L} \int_{-L}^L R dx \right) - k_1 k_2 \frac{RC^2}{C^2 + k_3^2}, & (x, t) \in (-L, L) \times (0, T), \\ C_t = C_{xx} + R - C, & (x, t) \in (-L, L) \times (0, T), \\ R_x(x, t) = C_x(x, t) = 0, & x = -L, L, t \in (0, T), \\ R(x, t) = R_0(x, t), & (x, t) \in (-L, L) \times [-\tau, 0], \\ C(x, 0) = C_0(x), & x \in (-L, L). \end{cases} \tag{4.1}$$

We shall show that spatiotemporal pattern formation is possible for (4.1) as a combined effect of diffusion, kinetic dynamics as shown in Sect. 3, and also the nonlocal integral term.

It is easy to see that a steady state  $(R_*, R_*)$  of (3.1) is a constant steady state solution of (4.1). Linearizing Eq. (4.1) at a constant steady state  $(R_*, R_*)$ , we obtain the following eigenvalue problem which determines the linear stability of the constant steady state:

$$\begin{cases} \mu\phi = D\phi_{xx} + (k_1 R_* f'_1(R_*) + k_1 R_*^\alpha) \phi - k_1 R_* f'_2(R_*)\psi - k_1 R_*^\alpha \frac{1}{2L} \int_{-L}^L \phi dx, & x \in (-L, L), \\ \mu\psi = \psi_{xx} + \phi - \psi, & x \in (-L, L), \\ \phi_x(x) = \psi_x(x) = 0, & x = -L, L, \end{cases} \tag{4.2}$$

where  $f_1(R)$  and  $f_2(R)$  are defined in (3.6). The eigenvalue problem (4.2) can be considered in the real-valued Sobolev space with the Neumann Boundary problem  $X = \{(\phi, \psi) \in H^2(-L, L) \times H^2(-L, L) : R_x(\pm L) = C_x(\pm L) = 0\}$ , and the eigenvalues of the corresponding diffusion operator  $u \mapsto -u''$  are

$$\lambda_n = \left(\frac{n\pi}{2L}\right)^2, \quad n \in \mathbb{N}_0 := \{0, 1, 2, \dots\}, \tag{4.3}$$

and the corresponding eigenfunctions are

$$\varphi_n(x) = \begin{cases} \cos(\sqrt{\lambda_n}x), & n = 0, 2, 4, \dots, \\ \sin(\sqrt{\lambda_n}x), & n = 1, 3, 5, \dots \end{cases} \tag{4.4}$$

The following lemma shows that the eigenvalue problem (4.2) can be solved through a Fourier decomposition of the eigenfunctions and it is reduced to eigenvalues of infinitely many  $2 \times 2$  matrices.

**Lemma 4.1** *Let  $\lambda_n$  and  $\varphi_n(x)$  be defined by (4.3) and (4.4) respectively, and let  $(R_*, R_*)$  be a constant steady state of Eq. (4.1) with  $R_*$  satisfying Eq. (3.4). Define*

$$\begin{aligned} J_0 &= \begin{pmatrix} k_1 R_* f'_1(R_*) & -k_1 R_* f'_2(R_*) \\ 1 & -1 \end{pmatrix}, \\ J_n &= \begin{pmatrix} -D\lambda_n + k_1 R_* f'_1(R_*) + k_1 R_*^\alpha & -k_1 R_* f'_2(R_*) \\ 1 & -\lambda_n - 1 \end{pmatrix}, \quad n = 1, 2, 3, \dots, \end{aligned} \tag{4.5}$$

then we have

- (i) if  $\mu$  is an eigenvalue of (4.2), then there exists  $n \in \mathbb{N}_0$  such that  $\mu$  is an eigenvalue of  $J_n$ ;
- (ii)  $(R_*, R_*)$  is locally asymptotically stable when the eigenvalues of  $J_n$  for all  $n \in \mathbb{N}_0$  have negative real parts, and it is unstable when there exists some  $n \in \mathbb{N}_0$  such that  $J_n$  has at least one eigenvalue with positive real part.

**Proof** By the Fourier expansion, we can write the eigenfunction of (4.2) as

$$(\phi, \psi)^T = \sum_{n=0}^{\infty} (a_n, b_n)^T \varphi_n(x). \tag{4.6}$$

Substituting (4.6) into (4.2), multiplying both sides by  $\varphi_n(x)$  and integrating the equations on  $[-L, L]$ , then by using the orthogonality of  $\varphi_n(x)$ , we obtain that

$$J_n(a_n, b_n)^T = \mu(a_n, b_n)^T, \text{ for } n \in \mathbb{N}_0.$$

Note that the nonlocal term

$$\int_{-L}^L \phi(x)dx = \int_{-L}^L \sum_{n=0}^{\infty} a_n \varphi_n(x)dx = \begin{cases} a_0, & n = 0; \\ 0, & n = 1, 2, \dots \end{cases},$$

so  $J_0$  is different from other  $J_n$  with  $n \geq 1$ . Therefore, we know that the eigenvalues of (4.2) are identical with those of the matrix  $J_n$  ( $n \in \mathbb{N}_0$ ), so the stability of the constant equilibrium  $(R_*, R_*)$  is determined by the eigenvalues of  $J_n$ . By (Simonett 1995, Theorem 8.6)  $(R_*, R_*)$  is locally asymptotically stable when the real parts of all the eigenvalues of  $J_n$  ( $n \in \mathbb{N}_0$ ) are negative and, it is unstable when there exists a  $J_n$  with eigenvalues of positive real part. □

From Lemma 4.1, the eigenvalues of (4.2) are the eigenvalues of  $J_n$ , which are determined by the characteristic equation

$$\Gamma_n(\mu) = \mu^2 - T_n\mu + D_n = 0, \tag{4.7}$$

where

$$T_0 = k_1 R_* f_1'(R_*) - 1, \quad D_0 = k_1 R_* (f_2'(R_*) - f_1'(R_*)),$$

and for  $n \geq 1$ ,

$$T_n = -(D + 1)\lambda_n + k_1 R_* f_1'(R_*) + k_1 R_*^\alpha - 1, \\ D_n = D\lambda_n^2 + (D - k_1 R_* f_1'(R_*) - k_1 R_*^\alpha)\lambda_n + k_1 R_* (f_2'(R_*) - f_1'(R_*)) - k_1 R_*^\alpha.$$

Following the approach in Wang et al. (2011) and Yi et al. (2009), the condition for the occurrence of a Hopf bifurcation near  $(R_*, R_*)$  is that there exist a pair of purely imaginary eigenvalues  $\pm i\omega_n$  with  $\omega_n > 0$  such that Eq. (4.7) holds, which is equivalent to that there exists  $n \in \mathbb{N}_0$  such that

$$(H) \quad T_n = 0, D_n > 0, \text{ and } T_i \neq 0, D_i \neq 0 \text{ for } i \neq n.$$

Also, we need to verify the transversality condition which is  $\frac{dRe(\mu)}{dk_1} \neq 0$  for Hopf bifurcation. By the fact that  $Re(\mu) = T_n/2$ , we obtain that

$$\frac{dRe(\mu)}{dk_1} = R_* f_1'(R_*) + R_*^\alpha = (\alpha - 1)R_*^{\alpha-1}(1 - R_*) > 0,$$

because  $0 < R_* < 1$ . Therefore, the transversality condition holds and a Hopf bifurcations indeed occurs at the following defined bifurcation points.

Here we choose  $k_1$  as the bifurcation parameter, while one can also use other parameter as the bifurcation parameter. Then we have the spatially homogeneous

Hopf bifurcation point (which indeed is the Hopf bifurcation point of kinetic system (3.1), and thus the bifurcating periodic orbits are spatially homogeneous), and spatially non-homogeneous Hopf bifurcation points (where the bifurcating periodic orbits are spatially non-homogeneous) expressed by:

$$k_{1H}^{(0)} = \frac{1}{R_* f_1'(R_*)}, \quad k_{1H}^{(n)} = \frac{1 + (D + 1)\lambda_n}{R_* f_1'(R_*) + R_*^\alpha}, \quad n \in \mathbb{N}, \tag{4.8}$$

provided that  $k_2 \in (k_2^*, +\infty)$  such that  $R_* f_1'(R_*) > 0$  which is necessary for the homogeneous Hopf bifurcation, where

$$k_2^* = k_2 \left( \frac{\alpha - 1}{\alpha} \right) = \frac{(\alpha - 1)^{\alpha-3}}{\alpha^\alpha} \left[ (\alpha - 1)^2 + k_3^2 \alpha^2 \right], \tag{4.9}$$

with  $k_2(R)$  defined by (3.9). Also, notice that  $R_* f_1'(R_*) + R_*^\alpha = (\alpha - 1)R_*^{\alpha-1}(1 - R_*) > 0$  holds for any  $R_* \in (0, 1)$ , thus  $k_{1H}^{(n)} > 0$ . To sum up the discussion, we have the following lemma.

**Lemma 4.2** *For fixed parameters  $k_3, D$  in system (4.1) and let  $k_2^*$  and  $k_{1H}^{(n)}, n \in \mathbb{N}_0$  be defined by (4.9) and (4.8) respectively, then we have*

- (i) *when  $k_2 \in (0, k_2^*)$ , the spatially homogeneous Hopf bifurcation does not occur, but system (4.1) undergoes a spatially non-homogeneous Hopf bifurcation at  $k_1 = k_{1H}^{(n)}$  defined in (4.8) for each  $n \in \mathbb{N}$ ;*
- (ii) *when  $k_2 \in (k_2^*, +\infty)$ , system (4.1) undergoes a spatially homogeneous Hopf bifurcation at  $k_1 = k_{1H}^{(0)}$  and a spatially non-homogeneous Hopf bifurcation at  $k_1 = k_{1H}^{(n)}$  for each  $n \in \mathbb{N}$ .*

Similarly a steady state bifurcation occurs when

$$(S) \quad D_n = 0, T_n \neq 0, \text{ and } T_i \neq 0, D_i \neq 0, \text{ for } i \neq n,$$

holds for some  $n \in \mathbb{N}$ , which is also called the diffusion-driven instability developed by Turing (1952). According to the condition (S), by taking  $k_1$  as the bifurcation parameter, we can obtain the following bifurcation points for the Turing instability:

$$k_{1S}^{(n)} = \frac{D(\lambda_n^2 + \lambda_n)}{(R_* f_1'(R_*) + R_*^\alpha)\lambda_n + R_*(f_1'(R_*) - f_2'(R_*)) + R_*^\alpha}, \quad n \in \mathbb{N}. \tag{4.10}$$

Note that  $k_{1S}^{(n)}$  may not be positive, but there exist an  $N \in \mathbb{N}$  such that  $k_{1S}^{(n)} > 0$  when  $n > N$  and a steady state bifurcation indeed occurs at  $k_1 = k_{1S}^{(n)}$  when  $n > N$ . According to Yi et al. (2009), we also need to verify the transversality condition which is  $\frac{dD_n}{dk_1} \neq 0$  for the steady state bifurcation. By a direct calculation, we have

$$\frac{dD_n}{dk_1} = -(R_* f_1'(R_*) + R_*^\alpha)\lambda_n + R_*(f_2'(R_*) - f_1'(R_*) - R^{\alpha-1}) < 0,$$

thus the transversality condition is satisfied.

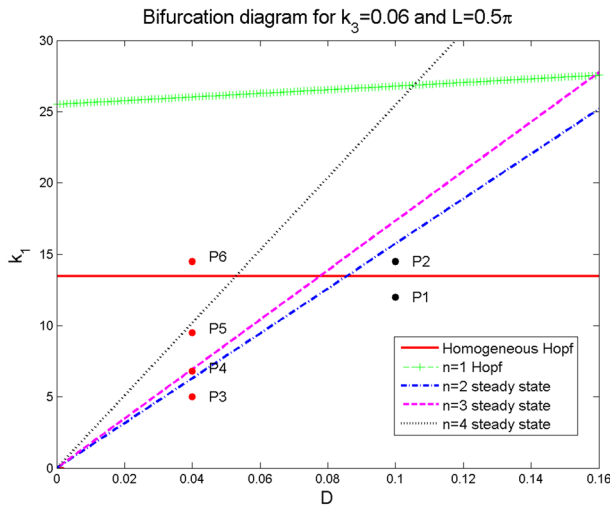


**Fig. 12** Steady state and Hopf bifurcation diagram for Eq. (4.1) on  $D - k_1$  plane with  $k_2 = 1, k_3 = 0.06, \alpha = 1.5, L = 0.5\pi$ . We choose six points in  $D - k_1$  plane to perform the numerical simulations:  $P1 = (0.1, 12), P2 = (0.1, 14.5), P3 = (0.04, 5), P4 = (0.04, 7), P5 = (0.04, 9.5), P6 = (0.04, 14.5)$

The Hopf bifurcation points defined in (4.8) and the steady state bifurcation points defined in (4.10) provide theoretical parameter values where spatial/temporal patterns for system (4.1) can emerge. In the remaining part of this section, we take some different values of  $k_1, D$  and the spatial domain length  $L$  to numerically demonstrate possible bifurcations and rich dynamical behavior of model (4.1).

**Example 4.3** We choose  $k_2 = 1, k_3 = 0.06, \alpha = 1.5, L = 0.5\pi$ . According to Proposition 3.4 and Fig. 4, there is a unique constant steady state  $(R_*, R_*) = (0.0259, 0.0259)$  which is determined by Eq. (3.4). According to Proposition 3.4,  $(0.0259, 0.0259)$  is locally asymptotically stable for  $k_1 \in (0, k_1^*)$  and unstable for  $k_1 \in (k_1^*, +\infty)$  with  $k_1^* = 13.4744$  being the homogeneous Hopf bifurcation point of the kinetic system (3.5). Then, by (4.8) and (4.10), we can compute the bifurcation points as

$$k_{1H}^{(0)} = k_1^* = 13.4744, k_{1H}^{(n)} = 12.7578(1 + (D + 1)n^2), k_{1S}^{(n)} = \frac{D(n^4 + n^2)}{0.0784n^2 - 0.1822}. \tag{4.11}$$

The bifurcation curves in (4.11) are plotted in Fig. 12 in  $D - k_1$  plane, and this diagram serves as a guidance map for the different spatiotemporal patterns shown below. Figure 13 demonstrates the situation when  $D = 0.1$  and  $k_1 = 12$  ( $P1$ ) or  $k_1 = 14.5$  ( $P2$ ) in Fig. 12. For parameter value at  $P1$ , the constant steady state  $(0.0259, 0.0259)$  is locally stable under a small random perturbation around the steady state (Fig. 13 upper row); while a spatially homogeneous time-periodic orbit arises when  $k_1$  crosses the homogeneous Hopf bifurcation line  $k_1 = k_{1H}^{(0)}$  and reaches  $P2$  (Fig. 13 lower row).

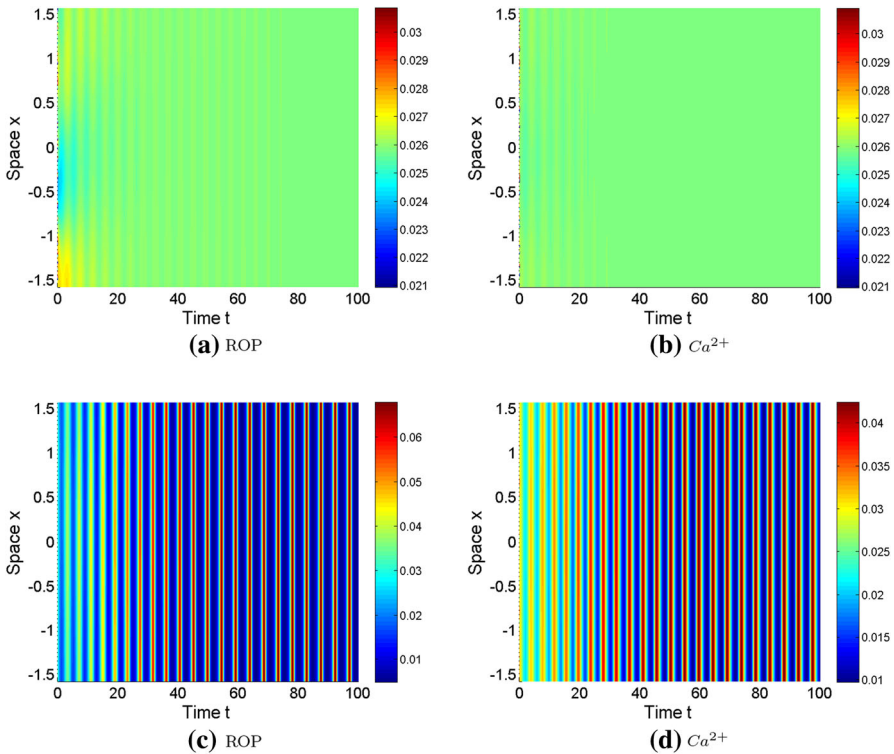


**Fig. 13** The dynamics of Eq. (4.1) when  $D = 0.1$ ,  $k_2 = 1$ ,  $k_3 = 0.06$ ,  $L = 0.5\pi$ . (Upper row:  $P1(0.1, 12)$ ):  $(R_*, R_*)$  remains stable; (Lower row:  $P2(0.1, 14.5)$ ): stable spatially homogeneous time-periodic pattern is observed. The initial condition is a small random perturbation of  $(0.0259, 0.0259)$

For a smaller diffusion rate  $D = 0.04$ , spatially non-homogeneous steady states and periodic orbits can be generated when  $k_1$  increases (see from Fig. 12). When  $k_1 = 5$  ( $P3$ ), the constant steady state is stable under a small perturbation (see Fig. 14 upper row); when  $k_1 = 7$  ( $P4$ ), a mode-2 Turing pattern (spatially non-homogeneous steady state) is observed (see the Fig. 14 middle row); and when  $k_1 = 9.5$  ( $P5$ ), a mode-3 Turing pattern is observed (see the Fig. 14 lower row). Finally if  $k_1$  crosses the homogeneous Hopf bifurcation line  $k_1 = k_{1H}^{(0)}$  to  $k_1 = 14.5$  ( $P6$ ), then spatiotemporal patterns (spatially non-homogeneous periodic orbits) are observed (see Fig. 15). Indeed by taking different initial values, two different patterns can be observed: a mode-3 spatiotemporal oscillating patterns is observed when a small random perturbation of the steady state is chosen as the initial condition (upper row), and a mode-4 spatiotemporal oscillating pattern is observed when the initial condition a prescribed one (lower row).

In this example, the homogeneous Hopf bifurcation curve ( $n = 0$ ) and the steady state bifurcation curve with lowest  $n$  ( $n = 2$ ) are where stability switches occur. For parameter values below both curves ( $P1, P3$ ), the constant steady state is stable; for the one above the homogeneous Hopf bifurcation curve but below the steady state

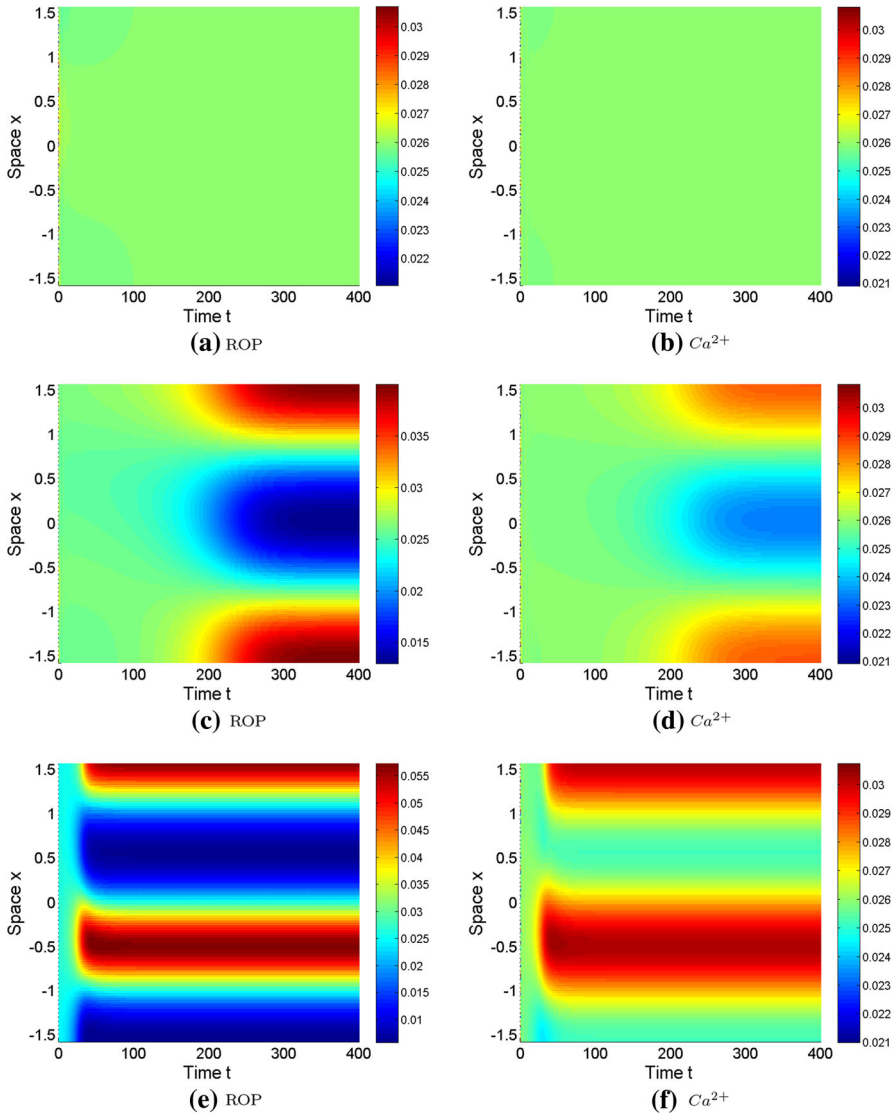


**Fig. 14** The dynamics of Eq. (4.1) when  $D = 0.04$ ,  $k_2 = 1$ ,  $k_3 = 0.06$ ,  $L = 0.5\pi$ . (Upper row:  $P3(0.04, 5)$ ): constant steady state; (Middle row:  $P4(0.04, 7)$ ): spatially non-homogeneous steady state with one peak ( $n = 2$ ); (Lower row:  $P5(0.04, 9.5)$ ): spatially non-homogeneous steady state with one and a half peaks ( $n = 3$ ))

bifurcation curve ( $P2$ ), a spatial homogeneous periodic orbit is observed; for the ones below the homogeneous Hopf bifurcation curve but above the steady state bifurcation curve ( $P4, P5$ ), a spatially non-homogeneous steady state is observed (number of peaks varies with different parameters); and for the one above both bifurcation curves ( $P6$ ), a spatially non-homogeneous periodic orbit emerges.

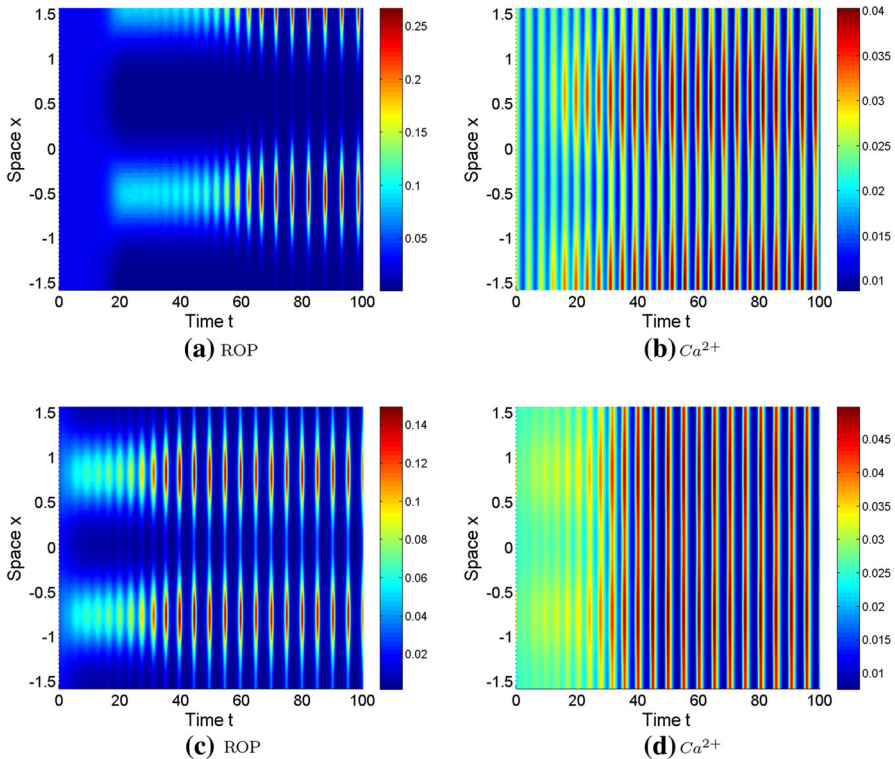


**Fig. 15** The dynamics of Eq. (4.1) when  $D = 0.04$ ,  $k_2 = 1$ ,  $k_3 = 0.06$ ,  $L = 0.5\pi : P6(0.04, 14.5)$ . (Upper row): the initial condition is a small random perturbation of  $(0.0259, 0.0259)$ ; (Lower row): the initial condition is  $(0.0259 - 0.01 \cos(4x), 0.0259 - 0.01 \cos(4x))$

**Example 4.4** We choose  $k_2 = 1$ ,  $k_3 = 0.5$ ,  $\alpha = 1.5$ ,  $L = \pi$ , according to Proposition 3.4 and Fig. 4, there is a unique steady state  $(R_*, R_*) = (0.3920, 0.3920)$  which is determined by Eq. (3.4) and is locally asymptotically stable for the kinetic system (3.1) by Proposition 3.4. Then, by (4.8) and (4.10), we can compute the bifurcation point as

$$k_{1H}^{(n)} = 5.2539(1 + (D + 1)n^2), \quad k_{1S}^{(n)} = \frac{D(n^4 + n^2)}{0.1903n^2 - 0.2812}. \tag{4.12}$$

Similarly, by plotting (4.12) in  $D - k_1$  plane, we obtain the bifurcation diagram in Fig. 16. Note that here a homogeneous Hopf bifurcation line is absent as  $k_2 < k_2^*$ . According to Lemma 4.2, we know that there is no homogeneous Hopf bifurcation in this case. When  $D = 0.2$ , Fig. 17 shows that the constant steady state is stable below the non-homogeneous Hopf bifurcation line ( $P7$ , upper row of Fig. 17), and a stable spatially non-homogeneous time-periodic pattern emerges when  $k_1$  crosses the first non-homogeneous Hopf bifurcation line ( $P8$ , lower row of Fig. 17). On the other hand when  $D = 0.1$ , with the increase of  $k_1$ , the first bifurcation line is the steady state bifurcation with mode  $n = 4$ , so we observe the spatially non-homogeneous

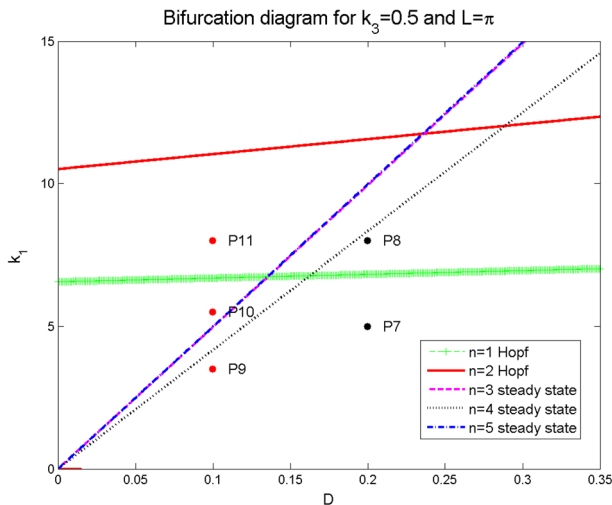


**Fig. 16** Steady state and Hopf bifurcation diagram for Eq. (4.1) on  $D-k_1$  plane with  $k_2 = 1$ ,  $k_3 = 0.5$ ,  $\alpha = 1.5$ ,  $L = \pi$ . In different regions, the dynamics of system (4.1) are different, and we select a point from each region to show the pattern formation of (4.1):  $P7 = (0.2, 5)$ , constant steady state;  $P8 = (0.2, 8)$ , mode-1 spatially non-homogeneous periodic patterns;  $P9 = (0.1, 3.5)$ , constant steady state;  $P10 = (0.1, 6)$ , spatially non-homogeneous steady state;  $P11 = (0.1, 8)$ , spatially non-homogeneous periodic patterns

steady state at  $P10$  (see the middle row of Fig. 18). Then the lower row of Fig. 18 demonstrates that a spatiotemporal oscillatory pattern is generated after  $k_1$  traverses the spatially non-homogeneous Hopf bifurcation line.

In this example, a spatially homogeneous Hopf bifurcation does not occur, and the spatially non-homogeneous time-periodic orbits can bifurcate directly from a constant steady state (Fig. 17), or through a steady state bifurcation first then a Hopf bifurcation (see Fig. 18), which is different from the ones in Example 4.3. Another interesting observation is that in Example 4.3, the peaks of spatially non-homogeneous time-periodic orbits are synchronized (see Fig. 19 upper row), while for Example 4.4, the peaks of spatially non-homogeneous time-periodic orbits are not synchronous (see Fig. 19 lower row). Indeed in latter case, the pattern oscillates with a swinging pattern with peak appearing alternatively on the left and right sides.

## 5 Conclusion

Oscillatory spatiotemporal  $Ca^{2+}$  signals have been observed in experiments, and it is identified as an important driving force of the polar cell growth in *Arabidopsis* pollen tubes (Luo et al. 2017). We propose a new reaction-diffusion model of ROP1 and  $Ca^{2+}$  interaction on the plasma membrane which incorporates positive feedback of ROP1, negative feedbacks between ROP1, and  $Ca^{2+}$ , lateral diffusive movement of ROP1 and  $Ca^{2+}$ . Mathematical analysis and numerical simulation of the system are conducted for (i) the non-spatial model without diffusion and time-delay; and (ii)

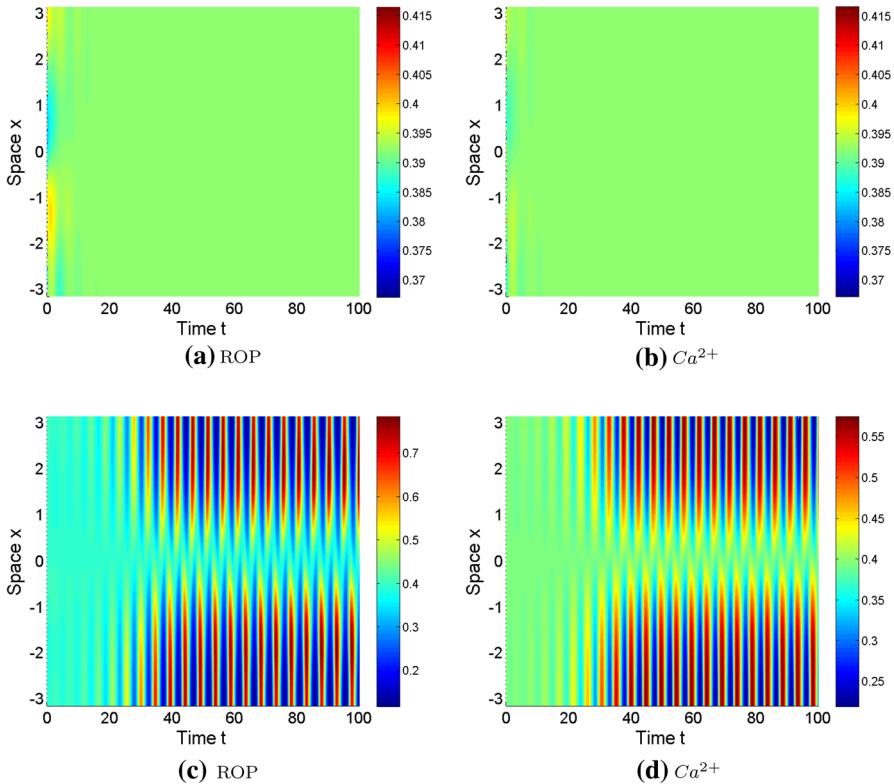


**Fig. 17** The dynamics of Eq. (4.1) when  $D = 0.2$ ,  $k_2 = 1$ ,  $k_3 = 0.5$ ,  $L = \pi$ . (Upper row:  $P7(0.2, 5)$ ): stable constant steady state; (Lower row:  $P8(0.2, 8)$ ): spatiotemporal pattern generated by spatially non-homogeneous Hopf bifurcation with  $n = 1$

the spatial model with diffusion, nonlocal effect but without time-delay. The effect of time-delay is not considered in this paper but will be analyzed in a future work.

It is revealed from mathematical analysis that the non-spatial model could have multiple steady states because of the degeneracy of the trivial steady state, and also the Hill type rate function that Calcium inhibits ROP1. Oscillations also occur in the non-spatial model as a result of Hopf bifurcation (steady state losing stability to temporal oscillation). The study of non-spatial models provides a guidance for parameter selection when detecting spatiotemporal patterns in spatial models. For the spatial reaction-diffusion model, parameter ranges supporting spatially non-homogenous time-periodic solutions are identified via linear stability analysis, and numerical simulations confirm the existence of stable spatially non-homogenous time-periodic patterns. Some of these patterns show a symmetric spatial profile with peak values occurring at two locations, and the peak values oscillates with the time. These spatiotemporal characters qualitatively match with experimental data from Yang's lab (Hwang et al. 2005). Quantitative comparison of numerical simulated solutions and experimental data, model validation using experimental data as well as fine tuning of the reaction-diffusion model will be the next stage of the investigation.

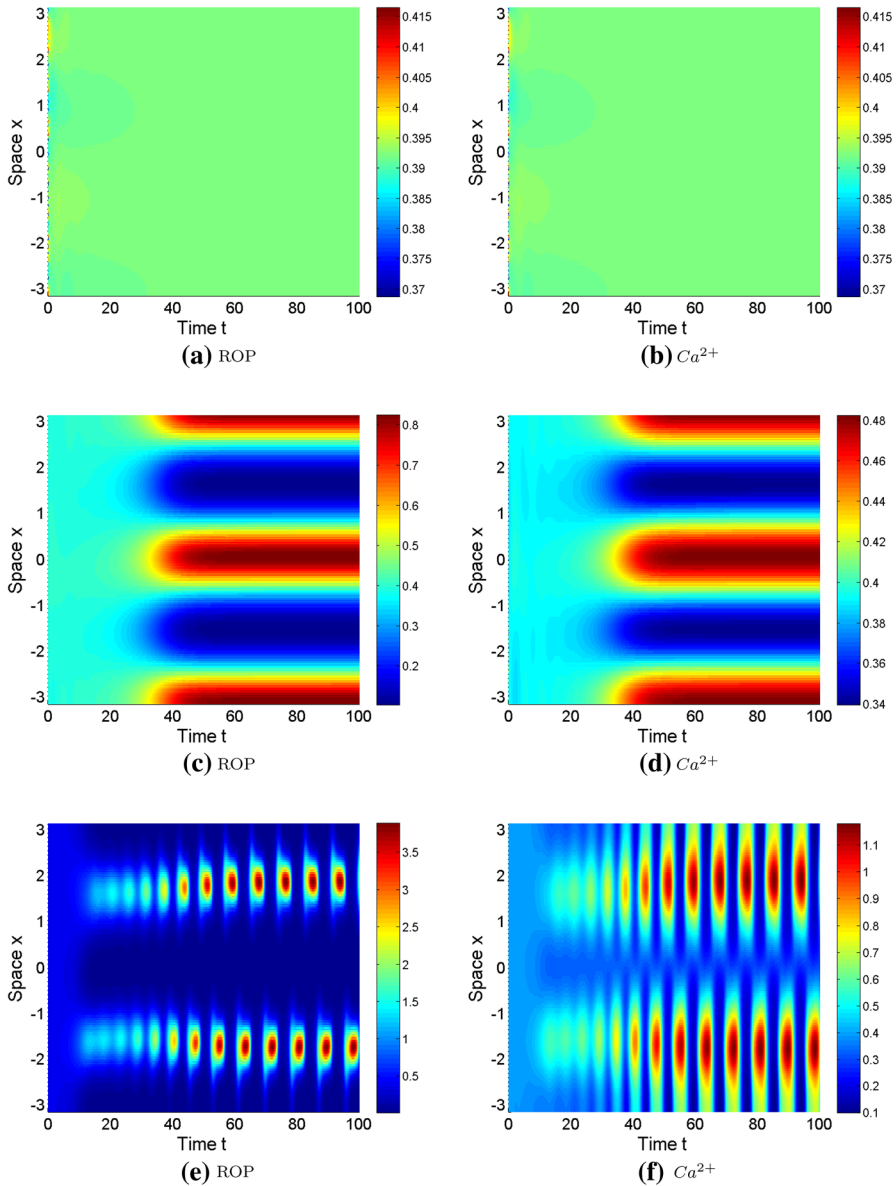


**Fig. 18** The dynamics of Eq. (4.1) when  $D = 0.1$ ,  $k_2 = 1$ ,  $k_3 = 0.5$ ,  $L = \pi$ . (Upper row:  $P9(0.1, 3.5)$ ): stable constant steady state; (Middle row:  $P10(0.1, 6)$ ): spatially non-homogeneous steady state with two peaks; (Lower row:  $P11(0.1, 8)$ ): spatiotemporal pattern with two peaks

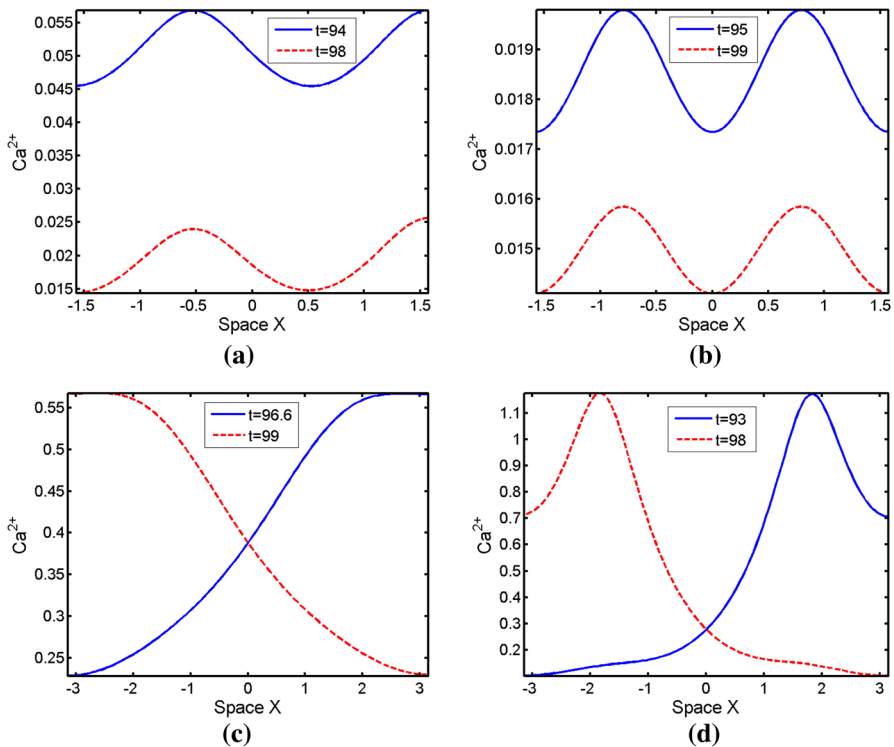


**Fig. 19** The snapshots of the spatiotemporal patterns of  $Ca^{2+}$  at certain moments. (Upper row): **a** the snapshots of patterns in Fig. 15a; **b** the snapshots of patterns in Fig. 15c. (Lower row): **c** the snapshots of patterns in Fig. 17c; **d** the snapshots of patterns in Fig. 18e

The spatiotemporal pattern formation discovered here also extends the classical Turing diffusion-induced pattern formation theory. In the standard reaction-diffusion system, a spatially non-homogenous time-periodic solution bifurcating from a trivial steady state is usually not stable, as the only stable time-periodic solution would be the spatially homogenous one. Here we find that the presence of a nonlocal integral term (in the model it represents the total amount of cytoplasmic molecules) could change this. In our model, a spatially non-homogenous time-periodic solution could be the first bifurcating pattern from a stable homogeneous steady state, hence it could be a stable pattern. Theoretical study in that aspect will be continued in another work (Shi et al. 2019a) for more general situations.

In this paper a spatiotemporal mathematical model in a one-dimensional spatial domain is considered, while a more realistic model for the interaction between ROP1 and  $Ca^{2+}$  is on a two-dimensional or three-dimensional spatial domain. The simplified one-dimensional model here illustrates the reaction-diffusion pattern formation mechanism, and we expect similar spatiotemporal patterns also occur in the more realistic two-dimensional or three-dimensional models. This will be verified in our future work.

## 6 Appendix

**Proof of Proposition 3.1** In this proposition, we study the number of roots of equation (3.4) with  $1 < \alpha < 2$ . The function  $f(R)$  has the properties that

$$\lim_{R \rightarrow 0^+} f(R) = -\infty \quad \text{and} \quad \lim_{R \rightarrow \infty} f(R) = \infty. \quad (6.1)$$

Also, we have the first derivative of  $f(R)$  as

$$f'(R) = \alpha R^{\alpha-1} - (\alpha - 1)R^{\alpha-2} + k_3^2(\alpha - 2)R^{\alpha-3} - k_3^2(\alpha - 3)R^{\alpha-4}. \quad (6.2)$$

Let

$$h(R) = \alpha R^3 - (\alpha - 1)R^2 + k_3^2(\alpha - 2)R - k_3^2(\alpha - 3). \quad (6.3)$$

So we have  $f'(R) = R^{\alpha-4}h(R)$ .

**Step 1.** There exists a unique  $x_2 > 0$  such that  $h'(R) < 0$  for  $0 < R < x_2$ ,  $h'(R) > 0$  for  $R > x_2$ , and  $h(R)$  reaches the global minimum in  $(0, \infty)$  at  $R = x_2$ .

Note that the function  $h(R)$  has the properties that

$$h(0) = -k_3^2(\alpha - 3) > 0 \quad \text{and} \quad \lim_{R \rightarrow \infty} h(R) = \infty, \quad (6.4)$$

and we have the first derivative of  $h(R)$  as

$$h'(R) = 3\alpha R^2 - 2(\alpha - 1)R + k_3^2(\alpha - 2). \quad (6.5)$$

Since  $\alpha \in (1, 2)$ , for (6.5), we have the discriminant  $\Delta_1 = 4(\alpha - 1)^2 - 12k_3^2\alpha(\alpha - 2) > 0$ . In this case,  $h'(R) = 0$  must have two roots in  $(-\infty, \infty)$ . Notice that  $\frac{2(\alpha - 1)}{3\alpha} > 0$  and  $\frac{k_3^2(\alpha - 2)}{3\alpha} < 0$  so  $h'(R)$  must have one negative root and one positive root. Let  $x_2$  be the positive root of  $h'(R) = 0$ . Since  $h'(0) = k_3^2(\alpha - 2) < 0$ , we have  $h'(R) < 0$  for  $0 < R < x_2$ ,  $h'(R) > 0$  for  $R > x_2$ . Therefore,  $h(R)$  decreases for  $0 < R < x_2$ , and increases for  $R > x_2$ . That is to say, if  $h(x_2) \geq 0$ , then  $h(R) \geq 0$  for any  $R > 0$ , while  $h(R) = 0$  has two positive solutions if  $h(x_2) < 0$ .

**Step 2.** There exist  $k_{31}, k_{32} > 0$  such that

$$h(x_2) \begin{cases} \geq 0, & \text{if } k_{31} < k_3 < k_{32}. \\ < 0, & \text{if } 0 < k_3 < k_{31} \text{ or } k_3 > k_{32}. \end{cases} \quad (6.6)$$

Since  $h'(R)$  is an quadratic function and the relationship between  $h(R)$  and  $h'(R)$ , we can have following two facts:

$$x_2 = \frac{(\alpha - 1) + \sqrt{(\alpha - 1)^2 - 3k_3^2\alpha(\alpha - 2)}}{3\alpha}, \quad (6.7)$$

$$h(x_2) = \left(\frac{x_2}{3} - \frac{\alpha - 1}{9\alpha}\right)h'(x_2) + \frac{6k_3^2\alpha(\alpha - 2) - 2(\alpha - 1)^2}{9\alpha}x_2 + \frac{k_3^2(\alpha - 1)(\alpha - 2) - 9k_3^2\alpha(\alpha - 3)}{9\alpha}. \tag{6.8}$$

Therefore, we have

$$h(x_2) \geq 0 \tag{6.9}$$

$$\Leftrightarrow x_2 \leq \frac{(\alpha - 1)(\alpha - 2) - 9\alpha(\alpha - 3)}{2(\alpha - 1)^2 - 6k_3^2\alpha(\alpha - 2)}k_3^2 \tag{6.10}$$

$$\Leftrightarrow \frac{(\alpha - 1) + \sqrt{(\alpha - 1)^2 - 3k_3^2\alpha(\alpha - 2)}}{3\alpha} \leq \frac{(\alpha - 1)(\alpha - 2) - 9\alpha(\alpha - 3)}{2(\alpha - 1)^2 - 6k_3^2\alpha(\alpha - 2)}k_3^2 \tag{6.11}$$

$$\Leftrightarrow Ak_3^4 + Bk_3^2 + C \geq 0, \tag{6.12}$$

where

$$A = \alpha(\alpha - 2)^3 < 0, \tag{6.13}$$

$$B = 2(\alpha - 1)^2(\alpha - 2)^2 - 18(\alpha - 1)(\alpha - 2) + 27 > 0, \tag{6.14}$$

$$C = (\alpha - 1)^3(\alpha - 3) < 0. \tag{6.15}$$

Notice that the discriminant of the quadratic function  $Ay^2 + By + C$  is

$$\Delta_2 = [2(\alpha - 1)^2(\alpha - 2)^2 - 18(\alpha - 1)(\alpha - 2) + 27]^2 - 4\alpha(\alpha - 1)^3(\alpha - 2)^3(\alpha - 3) \tag{6.16}$$

$$= [2(\alpha - 1)^2(\alpha - 2)^2 - 18(\alpha - 1)(\alpha - 2) + 27]^2 - 4(\alpha - 1)^4(\alpha - 2)^4 + 8(\alpha - 1)^3(\alpha - 2)^3 \tag{6.17}$$

$$> -18(\alpha - 1)(\alpha - 2)[4(\alpha - 1)^2(\alpha - 2)^2 - 18(\alpha - 1)(\alpha - 2) + 27] + 8(\alpha - 1)^3(\alpha - 2)^3 \tag{6.18}$$

$$= -2(\alpha - 1)(\alpha - 2)[32(\alpha - 1)^2(\alpha - 2)^2 - 162(\alpha - 1)(\alpha - 2) + 243]. \tag{6.19}$$

Since the discriminant of the quadratic function  $32y^2 - 162y + 243$  is  $\Delta_3 = 162^2 - 4 \times 32 \times 243 = -4860 < 0$ , then  $32(\alpha - 1)^2(\alpha - 2)^2 - 162(\alpha - 1)(\alpha - 2) + 243 > 0$  for any  $\alpha$ . Therefore

$$\Delta_2 > -2(\alpha - 1)(\alpha - 2)[32(\alpha - 1)^2(\alpha - 2)^2 - 162(\alpha - 1)(\alpha - 2) + 243] > 0. \tag{6.20}$$

So the quadratic equation  $Ay^2 + By + C = 0$  has two real-valued solutions  $k_{31}^* < k_{32}^*$ .

Because  $k_{31}^* + k_{32}^* = -\frac{B}{A} > 0$  and  $k_{31}^*k_{32}^* = \frac{C}{A} > 0$ , then  $k_{31}^*$  and  $k_{32}^*$  are both positive.

Moreover we can have that  $Ak_3^4 + Bk_3^2 + C \geq 0$  if and only if  $k_{31}^* \leq k_3^2 \leq k_{32}^*$ . Now let  $k_{31} = \sqrt{k_{31}^*}$  and  $k_{32} = \sqrt{k_{32}^*}$ , we reach the conclusion in (6.6).

**Step 3.** We consider the number of roots of equation  $f(R) = 0$  in (3.4) for each case in (6.6). In the case where  $h(x_2) \geq 0$ , we would have  $h(R) \geq 0$  for any  $R > 0$  because  $h(R)$  decreases for  $0 < R < x_2$ , and increases for  $R > x_2$ . That is to say,  $f'(R) = R^{\alpha-4}h(R) > 0$  for any  $R > 0$ . So  $f(R)$  increases for all  $R > 0$ . According to property (6.1),  $f(R) = 0$  has one unique positive root.

On the other hand, when  $h(x_2) < 0$ ,  $h(R) = 0$  has two positive solutions. Let  $0 < r_1 < x_2 < r_2$  be the solutions of  $h(R) = 0$ . Then  $h(R) > 0$  if  $R \in [0, r_1) \cup (r_2, +\infty)$  and  $h(R) < 0$  if  $R \in (r_1, r_2)$ . That is to say,

$$f'(R) = R^{\alpha-4}h(R) \begin{cases} > 0, & \text{if } R \in (0, r_1), \\ < 0, & \text{if } R \in (r_1, r_2), \\ > 0, & \text{if } R \in (r_2, +\infty). \end{cases} \tag{6.21}$$

Therefore,  $f(R)$  increases for  $0 < R < r_1$ , decreases for  $r_1 < R < r_2$ , and increases when  $R > r_2$ . Then we know that

1. If  $f(r_1)f(r_2) > 0$ , then  $f(R) = 0$  has one unique positive solution.
2. If  $f(r_1)f(r_2) = 0$ , then  $f(R) = 0$  has two positive solutions.
3. If  $f(r_1)f(r_2) < 0$ , then  $f(R) = 0$  has three positive solutions.

Define

$$l(R) = R^{\alpha-3}(1 - R)(R^2 + k_3^2). \tag{6.22}$$

Then  $f(r_1)f(r_2) = [k_2 - l(r_1)][k_2 - l(r_2)]$ . Since  $r_1$  and  $r_2$  are solutions of  $h(R) = 0$ ,  $r_1$  and  $r_2$  only depends on  $\alpha$  and  $k_3$ . So there exists  $k_{21}, k_{22}$  which only depends on  $\alpha, k_3$  and are defined as

$$k_{21} = r_1^{\alpha-3}(1 - r_1)(r_1^2 + k_3^2), \quad k_{22} = r_2^{\alpha-3}(1 - r_2)(r_2^2 + k_3^2), \tag{6.23}$$

such that

1. If  $k_2 < k_{21}$  or  $k_2 > k_{22}$ , then  $f(R) = 0$  has one unique positive solution.
2. If  $k_2 = k_{21}$  or  $k_2 = k_{22}$ , then  $f(R) = 0$  has two positive solutions.
3. If  $k_{21} < k_2 < k_{22}$ , then  $f(R) = 0$  has three positive solutions.

We claim that  $0 < k_{21} < k_{22}$  for  $0 < k_3 < k_{31}$ , while  $k_{21} < k_{22} < 0$  for  $k_3 > k_{32}$ . This is equivalent to  $r_1 < r_2 < 1$  for  $0 < k_3 < k_{31}$ , while  $1 < r_1 < r_2$  for  $k_3 > k_{32}$ . Notice that  $h(1) = 1 + k_3^2 > 0$ , and that  $h(R)$  decreases for  $0 < R < x_2$  and increases for  $R > x_2$ . So we only need to prove that  $h'(1) = \alpha + 2 + k_3^2(\alpha - 2) < 0$  for  $0 < k_3 < k_{31}$ , while  $h'(1) > 0$  for  $k_3 > k_{32}$ . In fact,  $k_{31}^2$  and  $k_{32}^2$  are two positive roots of equation  $Ay^2 + By + C = 0$ , where  $A, B, C$  are defined as (6.13), (6.14) and (6.15) respectively. Notice that  $A < 0$  and

$$A \left( \frac{2 + \alpha}{2 - \alpha} \right)^2 + B \left( \frac{2 + \alpha}{2 - \alpha} \right) + C = 32 \left( \alpha - \frac{1}{4} \right)^2 + 54 \frac{\alpha}{2 - \alpha} > 0, \quad \text{for } 1 < \alpha < 2. \tag{6.24}$$

So  $k_{31}^2 < \frac{2 + \alpha}{2 - \alpha} < k_{32}^2$ . Therefore, we have

$$h'(1) = \alpha + 2 + k_3^2(\alpha - 2) > \alpha + 2 + k_{31}^2(\alpha - 2) > 0, \quad \text{if } 0 < k_3 < k_{31}, \quad (6.25)$$

$$h'(1) = \alpha + 2 + k_3^2(\alpha - 2) < \alpha + 2 + k_{32}^2(\alpha - 2) < 0, \quad \text{if } k_3 > k_{32}. \quad (6.26)$$

So we have proved that  $0 < k_{21} < k_{22}$  for  $0 < k_3 < k_{31}$ , while  $k_{21} < k_{22} < 0$  for  $k_3 > k_{32}$ . Therefore we reach the conclusion about number of solution of  $f(R) = 0$ . □

**Proof of Proposition 3.2** By the Center Manifold Theorem (Page 116 in Perko (2001)), we can compute the center manifold near the equilibrium  $(0, 0)$ :

$$C = \vartheta(R) = \frac{1}{k_1(2 - \alpha)} R^{2-\alpha} + o(R^{2-\alpha}). \quad (6.27)$$

Then, by substituting (6.27) into the first equation of the kinetic system (3.1), we obtain the following scalar system which gives the flow of Eq. (3.1) on the center manifold:

$$R_t = k_1 R^\alpha(1 - R) - k_1 k_2 \frac{R \vartheta^2(R)}{\vartheta^2(R) + k_3^2} > 0, \quad \text{for } 0 < R < \delta. \quad (6.28)$$

Thus, we know that the flow on the center manifold is moving away from the origin and it is an unstable orbit.

Next we show that there is an invariant region near  $R = 0, C > 0$  for Eq. (3.1). Define

$$O = \left\{ (R, C) : 0 \leq R \leq \left( \frac{k_2}{2(k_3^2 + \delta^2)} \right)^{\frac{1}{\alpha-1}} C^{\frac{2}{\alpha-1}}, 0 \leq C \leq \delta \right\}.$$

It is obvious that  $R = 0$  is invariant for (3.1). Then, if  $C = \delta, 0 \leq R \leq \left( \frac{k_2}{2(k_3^2 + \delta^2)} \right)^{\frac{1}{\alpha-1}} \delta^{\frac{2}{\alpha-1}}$ , since  $1 < \alpha < 2$  then  $\frac{2}{\alpha-1} > 1$ , so one can choose  $\delta > 0$

small enough so that  $\left( \frac{k_2}{2(k_3^2 + \delta^2)} \right)^{\frac{1}{\alpha-1}} \delta^{\frac{2}{\alpha-1}} \leq \delta$ . By using  $C = \delta$ , we have  $C' < 0$ .

On the boundary  $R = \left(\frac{k_2}{2(k_3^2 + \delta^2)}\right)^{\frac{1}{\alpha-1}} C^{\frac{2}{\alpha-1}}$ , we have

$$\begin{aligned} \frac{d}{dt} \left(\frac{R^{\frac{\alpha-1}{2}}}{C}\right) &= \frac{\frac{\alpha-1}{2}CR^{\frac{\alpha-3}{2}}R' - R^{\frac{\alpha-1}{2}}C'}{C^2} = \frac{R^{\frac{\alpha-3}{2}}}{C^2} \left(\frac{\alpha-1}{2}CR' - RC'\right) \\ &= \frac{R^{\frac{\alpha-3}{2}}}{C^2} \left[\frac{\alpha-1}{2}Ck_1 \left(R^\alpha - R^{\alpha+1} - k_2 \frac{RC^2}{C^2 + k_3^2}\right) - R^2 + CR\right] \\ &\leq \frac{R^{\frac{\alpha-3}{2}}}{C} \left[\frac{\alpha-1}{2}k_1 \left(R^\alpha - k_2 \frac{RC^2}{C^2 + k_3^2}\right) + R\right] \\ &\leq \frac{R^{\frac{\alpha-3}{2}}}{C} \left[(\alpha-1)k_1R^\alpha - \frac{(\alpha-1)k_1k_2RC^2}{2(C^2 + k_3^2)}\right] \\ &\leq \frac{R^{\frac{\alpha-3}{2}}}{C} \left[(\alpha-1)k_1 \left(R^\alpha - \frac{(\alpha-1)k_1k_2RC^2}{2(\delta^2 + k_3^2)}\right)\right] \\ &= (\alpha-1)R^{\frac{\alpha-1}{2}}k_1C^2 \left[\frac{R^{\alpha-1}}{C^2} - \frac{k_2}{2(\delta^2 + k_3^2)}\right] = 0, \end{aligned}$$

and the first inequality holds for  $R$  small enough:  $R < \frac{\alpha-1}{2}k_1R^\alpha$ . The above calculation implies that the dynamics of (3.1) is inward on  $R = \left(\frac{k_2}{2(k_3^2 + \delta^2)}\right)^{\frac{1}{\alpha-1}} C^{\frac{2}{\alpha-1}}$ . This shows that  $O$  is an invariant region for Eq. (3.1), and any orbit in  $O$  converges to the origin. It is also clear that when  $R = 0, C > 0$  (the positive  $C$ -axis), we have  $(R_t, C_t) = (0, -C)$ . So we know that all the solutions starting from  $R = 0, C > 0$  will always stay on this curve and eventually converge to the origin. One can choose a maximum orbit  $R = h_s(C)$  so that all orbits such that  $0 \leq R \leq h_s(C)$  converge to the origin. Then other trajectories exhibits saddle behavior near the origin.  $\square$

**Proof of Theorem 3.3** First, we look at the determinant of the Jacobian matrix  $J(R_j, R_j): \text{Det}(J(R_j, R_j)) = k_1R_j(f_2'(R_j) - f_1'(R_j))$ , where  $f_1, f_2$  are defined in (3.6). From (3.6), we have

$$f_2(R) - f_1(R) = \frac{k_2R^2}{R^2 + k_3^2} - R^{\alpha-1}(1 - R) \tag{6.29}$$

$$\Leftrightarrow f(R) = k_2 - R^{\alpha-3}(1 - R)(R^2 + k_3^2) = \frac{R^2 + k_3^2}{R^2}(f_2(R) - f_1(R)) \tag{6.30}$$

$$\Leftrightarrow f'(R) = -\frac{2k_3^2}{R^3}(f_2(R) - f_1(R)) + \frac{R^2 + k_3^2}{R^2}(f_2'(R) - f_1'(R)). \tag{6.31}$$

From (6.30), we know that  $f_2(R) - f_1(R) = 0$  when  $f(R) = 0$ . Since positive steady states  $(R_j, R_j) (j = 1, 2, 3)$  satisfy  $f(R_j) = 0$ , we have  $f_2(R_j) - f_1(R_j) = 0$ .

Therefore, from (6.31), we know

$$\begin{aligned} f'(R_j) > 0 &\Leftrightarrow f'_2(R_j) - f'_1(R_j) > 0 \Leftrightarrow \text{Det}(J(R_j, R_j)) > 0; \\ f'(R_j) = 0 &\Leftrightarrow f'_2(R_j) - f'_1(R_j) = 0 \Leftrightarrow \text{Det}(J(R_j, R_j)) = 0; \\ f'(R_j) < 0 &\Leftrightarrow f'_2(R_j) - f'_1(R_j) < 0 \Leftrightarrow \text{Det}(J(R_j, R_j)) < 0. \end{aligned}$$

According to the proof of Proposition 3.1, we have the following result of  $\text{Det}(J(R_j, R_j))$ : there exists a constant  $k_{31} > 0$  such that

1. If  $0 < k_3 < k_{31}$ , then there exists  $r_1$  and  $r_2$ , which are two positive solutions of  $h(R) = 0$ , such that
  - (a)  $f'(R) > 0 \Rightarrow \text{Det}(J(R, R)) > 0$  for  $R \in (0, r_1) \cup (r_2, 1)$ ;
  - (b)  $f'(R) < 0 \Rightarrow \text{Det}(J(R, R)) < 0$  for  $R \in (r_1, r_2)$ .
2. If  $k_{31} < k_3$ , then for any  $0 < R < 1$ , we always have  $f'(R) > 0 \Rightarrow \text{Det}(J(R, R)) > 0$ .

Here we want to point out that from (6.23), we have  $k_2(r_1) = k_{21}$  and  $k_2(r_2) = k_{22}$ .

Next we look at the trace of Jacobian matrix (3.5):  $\text{Tr}(J(R_j, C_j)) = k_1 R_j f'_1(R_j) -$

1. Define a new function

$$g(R) = R f'_1(R) = R^{\alpha-1}[(\alpha - 1) - \alpha R]. \tag{6.32}$$

We observe that  $g(R)$  has the following properties:

$$g(0) = 0, \quad g\left(\frac{\alpha - 1}{\alpha}\right) = 0, \quad \text{and} \quad \lim_{R \rightarrow \infty} g(R) = \infty. \tag{6.33}$$

Also we have the first derivative of  $g(R)$  as

$$g'(R) = R^{\alpha-2}[(\alpha - 1)^2 - \alpha^2 R]. \tag{6.34}$$

Hence the function  $g(R)$  increases for  $0 < R < \left(\frac{\alpha - 1}{\alpha}\right)^2$  and decreases for  $R > \left(\frac{\alpha - 1}{\alpha}\right)^2$ . So  $g(R)$  achieves its maximum at  $R = \left(\frac{\alpha - 1}{\alpha}\right)^2$  with  $g\left(\left(\frac{\alpha - 1}{\alpha}\right)^2\right) = \left(\frac{\alpha - 1}{\alpha}\right)^{2\alpha-1}$ .

Therefore we conclude that

1. If  $k_1 < \left(\frac{\alpha}{\alpha - 1}\right)^{2\alpha-1}$ , then

$$\text{Tr}(J(R, R)) = k_1 g(R) - 1 < \left(\frac{\alpha}{\alpha - 1}\right)^{2\alpha-1} \left(\frac{\alpha - 1}{\alpha}\right)^{2\alpha-1} - 1 = 0. \tag{6.35}$$

2. If  $k_1 > \left(\frac{\alpha}{\alpha - 1}\right)^{2\alpha - 1}$ , then there exists  $0 < \tilde{R}_1 < \tilde{R}_2$ , such that  $g(\tilde{R}_1) = g(\tilde{R}_2) = \frac{1}{k_1}$ . Therefore,

- (a) If  $\tilde{R}_1 < R < \tilde{R}_2$ , then  $\text{Tr}(J(R, R)) = k_1g(R) - 1 > k_1g(\tilde{R}_1) = 0$ .
- (b) If  $0 < R < \tilde{R}_1$  or  $\tilde{R}_2 < R < 1$ , then  $\text{Tr}(J(R, R)) = k_1g(R) - 1 < k_1g(\tilde{R}_1) = 0$ .

□

**Proof of Proposition 3.4** From the proof of Theorem 3.3, we can easily get Part 1 in Proposition 3.4. So here we only discuss Part 2: the case that  $0 < k_3 < k_{31}$ . Since  $\text{Det}(J(R_2, C_2)) < 0$ , the steady state  $(R_2, C_2)$  is always a saddle point. So we focus on the positive steady states  $(R_1, C_1)$  and  $(R_3, C_3)$ . To prove the results in Proposition 3.4, we need to determine the order of the possible bifurcation points:  $r_1, r_2, \tilde{R}_1$  and  $\tilde{R}_2$ , where  $r_1$  and  $r_2$  are the steady state bifurcation points satisfying  $h(r_1) = h(r_2) = 0$  with  $h(R)$  defined in (6.3), and  $\tilde{R}_1, \tilde{R}_2$  are possible Hopf bifurcation points satisfying  $g(\tilde{R}_1) = g(\tilde{R}_2) = 1/k_1$ . Then, by the results of Theorem 3.3, we can obtain the stability of each steady state.

First, we prove that  $g(r_1) > g(r_2)$  always holds. From the definition of  $h(R)$ , we know that

$$h(r_1) = \alpha r_1^3 - (\alpha - 1)r_1^2 + k_3^2(\alpha - 2)r_1 - k_3^2(\alpha\alpha - 3) = 0. \tag{6.36}$$

Multiplying (6.36) by  $r_1^{\alpha - 3}$ , we have

$$\alpha r_1^\alpha - (\alpha - 1)r_1^{\alpha - 1} + k_3^2(\alpha - 2)r_1^{\alpha - 2} - k_3^2(\alpha\alpha - 3)r_1^{\alpha - 3} = 0, \tag{6.37}$$

which together with  $g(r_1) = -\alpha r_1^\alpha + (\alpha - 1)r_1^{\alpha - 1}$  from (6.32) implies that

$$g(r_1) = k_3^2(\alpha - 2)r_1^{\alpha - 2} - k_3^2(\alpha - 3)r_1^{\alpha - 3}. \tag{6.38}$$

Define

$$G(R) = k_3^2(\alpha - 2)R^{\alpha - 2} - k_3^2(\alpha - 3)R^{\alpha - 3}, \quad R \in (0, 1), \quad \alpha \in (1, 2). \tag{6.39}$$

By direct calculation, we have  $G'(R) = k_3^2(\alpha - 2)^2R^{\alpha - 3} - k_3^2(\alpha - 3)^2R^{\alpha - 4}$  and  $G'(R) < 0$  for  $R \in \left(0, \left(\frac{\alpha - 3}{\alpha - 2}\right)^2\right) \supset (0, 1)$ . Therefore,  $G(R)$  is strictly decreasing for  $R \in (0, 1)$ . By the fact that  $0 < r_1 < r_2 < 1$ , immediately we reach the conclusion that  $g(r_1) > g(r_2)$ .

Now we consider the case that  $0 < k_3 < k_{31}$  which implies the existence of multiple steady states. For the convenience of discussion, we define

$$\tilde{g}(R) = g(R) - 1/k_1, \tag{6.40}$$

then we know that  $\tilde{g}$  has two zeros  $\tilde{R}_1$  and  $\tilde{R}_2$ . For the order of  $r_1, r_2, \tilde{R}_1$  and  $\tilde{R}_2$ , we have the following six possible situations:

- (i)  $r_1 < r_2 < \tilde{R}_1 < \tilde{R}_2$ . We show that this case will not happen. By the property of  $h(R)$ , it is not difficult to verify that  $h\left(\left(\frac{\alpha-1}{\alpha}\right)^2\right) > 0 = h(r_2)$ , so we know that  $\left(\frac{\alpha-1}{\alpha}\right)^2 < r_2$ . Because  $\left(\frac{\alpha-1}{\alpha}\right)^2$  is the maximum point of  $\tilde{g}(R)$  and  $\tilde{R}_1$  is the smallest root of  $\tilde{g}(R)$ , so we have  $\tilde{R}_1 < r_2$  which is a contradiction to the assumption.
- (ii)  $r_1 < \tilde{R}_1 < r_2 < \tilde{R}_2$ . By the fact that  $\tilde{g}(R) > 0$  for  $R \in (\tilde{R}_1, \tilde{R}_2)$  and  $g(R) < 0$  for  $R \in (0, \tilde{R}_1) \cup (\tilde{R}_2, 1)$ , it is easy to obtain that  $\tilde{g}(r_1) < 0$  since  $r_1 < \tilde{R}_1$ , which is equivalent to  $k_1 < 1/g(r_1)$ . Also, by  $\tilde{g}(r_2) > 0$ , we have  $k_1 > 1/g(r_2)$ . However, it has been proved that  $g(r_1) > g(r_2)$ , so the set  $(1/g(r_2), 1/g(r_1))$  is empty, which means that this case cannot happen.
- (iii)  $\tilde{R}_1 < r_1 < r_2 < \tilde{R}_2$  (see Fig. 7c). Because that  $r_1, r_2 \in (\tilde{R}_1, \tilde{R}_2)$ , so we have  $\tilde{g}(r_1) > 0$  and  $\tilde{g}(r_2) > 0$ , which is equivalent to  $k_1 > 1/g(r_2)$ . In this case, by Theorem 3.3, we know that Hopf bifurcations occur at both of  $(R_1, R_1)$  and  $(R_3, R_3)$ .
- (iv)  $\tilde{R}_1 < r_1 < \tilde{R}_2 < r_2$  (see Fig. 7d). By similar argument, since  $r_1 \in (\tilde{R}_1, \tilde{R}_2)$  and  $r_2 > \tilde{R}_2$ , we can obtain that  $\tilde{g}(r_1) > 0$  and  $\tilde{g}(r_2) < 0$  which imply that  $k_1 \in (1/g(r_1), 1/g(r_2))$ . In this case, from  $\tilde{R}_1 < r_1 < \tilde{R}_2 < r_2$  and Theorem 3.3, a Hopf bifurcation only occurs at  $(R_3, R_3)$  and does not occur at  $(R_1, R_1)$ .
- (v)  $r_1 < \tilde{R}_1 < \tilde{R}_2 < r_2$  (see Fig. 7e). Similarly, we have  $\tilde{g}(r_1) < 0$  and  $\tilde{g}(r_2) < 0$ , then it can be inferred that  $k_{11} < k_1 < 1/g(r_1)$ . In this case, no Hopf bifurcation can occur. Also, we have  $\left(\frac{\alpha-1}{\alpha}\right)^2 > r_1$  in this case, which will be used later.
- (vi)  $\tilde{R}_1 < \tilde{R}_2 < r_1 < r_2$  (see Fig. 7f). In this case, we still have  $k_{11} < k_1 < 1/g(r_1)$ , but the difference with case (v) is that  $\left(\frac{\alpha-1}{\alpha}\right)^2 < r_1$ . In this case, two Hopf bifurcations occur at  $(R_1, R_1)$ .

So in order to distinguish the last two cases, we define  $\tilde{k}_3$  to be the value of  $k_3$  such that  $r_1 = \left(\frac{\alpha-1}{\alpha}\right)^2$ , and it is easy to calculate that  $\tilde{k}_3$  is given by (3.16). So case (v) is for  $0 < k_3 < \tilde{k}_3$  which is equivalent to  $r_1 < \left(\frac{\alpha-1}{\alpha}\right)^2$  and case (vi) is for  $\tilde{k}_3 < k_3 < k_{31}$  which implies  $r_1 > \left(\frac{\alpha-1}{\alpha}\right)^2$ . Also we must have that  $\tilde{k}_3 < k_{31}$ . Suppose not, then first we assume that  $k_3 > k_{32}$ , then  $h(R) = 0$  has two positive solutions, but both of them should be bigger than 1 and here we have  $0 < R < 1$  which is a contradiction. If  $k_{31} < k_3 < k_{32}$ , then  $h(R) = 0$  has no roots, so it contradicts with the fact that  $h(R) = 0$  has one of positive roots at  $\left(\frac{\alpha-1}{\alpha}\right)^2 < 1$  when  $k_3 = \tilde{k}_3$ . Therefore, we can conclude that  $\tilde{k}_3 < k_{31}$ . Finally if  $0 < k_1 < k_{11}$ , then  $\tilde{g}(R)$  has no zeros,  $(R_1, R_1)$  and  $(R_3, R_3)$  are both always linearly stable and Hopf bifurcation will not occur, which is similar to (v) above.

In summary the case (c) is implied by (iii) above, case (d) is implied by (iv) above, case (e) is implied by (v) and the case of  $0 < k_1 < k_{11}$ , and case (f) is implied by (vi) above. The proof is completed. □

## References

- Altschuler SJ, Angenent SB, Wang Y, Wu LF (2008) On the spontaneous emergence of cell polarity. *Nature* 454(7206):886–889
- Busenberg S, Huang W-Z (1996) Stability and Hopf bifurcation for a population delay model with diffusion effects. *J Differ Equ* 124(1):80–107
- Chen S-S, Lou Y, Wei J-J (2018) Hopf bifurcation in a delayed reaction-diffusion-advection population model. *J Differ Equ* 264(8):5333–5359
- Chen S-S, Shi J-P (2012) Stability and Hopf bifurcation in a diffusive logistic population model with nonlocal delay effect. *J Differ Equ* 253(12):3440–3470
- Chen S-S, Shi J-P, Wei J-J (2013) Time delay-induced instabilities and Hopf bifurcations in general reaction-diffusion systems. *J Nonlinear Sci* 23(1):1–38
- Chen S-S, Shi J-P, Wei J-J (2014) Bifurcation analysis of the Gierer-Meinhardt system with a saturation in the activator production. *Appl Anal* 93(6):1115–1134
- Chen S-S, Yu J-S (2016a) Stability analysis of a reaction-diffusion equation with spatiotemporal delay and Dirichlet boundary condition. *J Dyn Differ Equ* 28(3–4):857–866
- Chen S-S, Yu J-S (2016b) Stability and bifurcations in a nonlocal delayed reaction-diffusion population model. *J Differ Equ* 260(1):218–240
- Chou C-S, Nie Q, Yi T-M (2008) Modeling robustness tradeoffs in yeast cell polarization induced by spatial gradients. *PLoS One* 3(9):e3103
- Ding D-Q, Shi J-P, Wang Y (2017) Bistability in a model of grassland and forest transition. *J Math Anal Appl* 451(2):1165–1178
- Edelstein-Keshet L, Holmes WR, Zajac M, Dutot M (2013) From simple to detailed models for cell polarization. *Philos Trans R Soc Lond B Biol Sci* 368(1629):20130003
- Feijó JA, Sainhas J, Holdaway-Clarke T, Cordeiro MS, Kunkel JG, Hepler PK (2001) Cellular oscillations and the regulation of growth: the pollen tube paradigm. *Bioessays* 23(1):86–94
- Gierer A, Meinhardt H (1972) A theory of biological pattern formation. *Biol Cybern* 12(1):30–39
- Goryachev AB, Pokhilko AV (2008) Dynamics of Cdc42 network embodies a Turing-type mechanism of yeast cell polarity. *FEBS Lett* 582(10):1437–1443
- Gu Y, Fu Y, Dowd P, Li S-D, Vernoud V, Gilroy S, Yang Z-B (2005) A rho family gtpase controls actin dynamics and tip growth via two counteracting downstream pathways in pollen tubes. *J Cell Biol* 169(1):127–138
- Guo S-J (2015) Stability and bifurcation in a reaction-diffusion model with nonlocal delay effect. *J Differ Equ* 259(4):1409–1448
- Holmes WR, Edelstein-Keshet L (2016) Analysis of a minimal Rho-GTPase circuit regulating cell shape. *Phys Biol* 13(4):046001
- Hwang J-U, Gu Y, Lee Y-J, Yang Z-B (2005) Oscillatory ROP GTPase activation leads the oscillatory polarized growth of pollen tubes. *Mol Biol Cell* 16(11):5385–5399
- Jilkine A, Marée AFM, Edelstein-Keshet L (2007) Mathematical model for spatial segregation of the Rho-family GTPases based on inhibitory crosstalk. *Bull Math Biol* 69(6):1943–1978
- Jin J-Y, Shi J-P, Wei J-J, Yi F-Q (2013) Bifurcations of patterned solutions in the diffusive Lengyel-Epstein system of CIMA chemical reactions. *Rocky Mt J Math* 43(5):1637–1674
- Kondo S, Miura T (2010) Reaction-diffusion model as a framework for understanding biological pattern formation. *Science* 329(5999):1616–1620
- Li H, Lin Y-K, Heath RM, Zhu M X, Yang Z-B (1999) Control of pollen tube tip growth by a rop gtpase-dependent pathway that leads to tip-localized calcium influx. *Plant Cell* 11(9):1731–1742
- Li X, Wang H, Zhang Z, Hastings A (2014) Mathematical analysis of coral reef models. *J Math Anal Appl* 416(1):352–373
- Lo W-C, Park H-O, Chou C-S (2014) Mathematical analysis of spontaneous emergence of cell polarity. *Bull Math Biol* 76(8):1835–1865
- Ludwig D, Jones DD, Holling CS (1978) Qualitative analysis of insect outbreak systems: the spruce budworm and forest. *J Anim Ecol* 47(1):315–332
- Luo N, Yan A et al (2017) Exocytosis-coordinated mechanisms for tip growth underlie pollen tube growth guidance. *Nat Commun* 8(1):1687
- Maini P, Painter K, Chau H (1997) Spatial pattern formation in chemical and biological systems. *J Chem Soc Faraday Trans* 93(20):3601–3610

- Mogilner A, Allard J, Wollman R (2012) Cell polarity: quantitative modeling as a tool in cell biology. *Science* 336(6078):175–179
- Moore TI, Chou C-S, Nie Q, Jeon NL, Yi T-M (2008) Robust spatial sensing of mating pheromone gradients by yeast cells. *PLoS One* 3(12):e3865
- Mori Y, Jilkine A, Edelstein-Keshet L (2011) Asymptotic and bifurcation analysis of wave-pinning in a reaction-diffusion model for cell polarization. *SIAM J Appl Math* 71(4):1401–1427
- Mummy PJ, Hastings A, Edwards HJ (2007) Thresholds and the resilience of Caribbean coral reefs. *Nature* 450(7166):98–101
- Perko L (2001) *Differential equations and dynamical systems*, texts in applied mathematics, vol 7, 3rd edn. Springer, New York
- Rätz A, Röger M (2012) Turing instabilities in a mathematical model for signaling networks. *J Math Biol* 65(6–7):1215–1244
- Scheffer M, Carpenter S, Foley JA, Folke C, Walker B (2001) Catastrophic shifts in ecosystems. *Nature* 413(6856):591–596
- Scheffer M, Hosper SH, Meijer ML, Moss B, Jeppesen E (1993) Alternative equilibria in shallow lakes. *Trends Ecol Evol* 8(8):275–279
- Seirin Lee S, Gaffney EA, Baker RE (2011) The dynamics of Turing patterns for morphogen-regulated growing domains with cellular response delays. *Bull Math Biol* 73(11):2527–2551
- Shi Q-Y, Shi J-P, Song Y-L (2017) Hopf bifurcation in a reaction-diffusion equation with distributed delay and Dirichlet boundary condition. *J Differ Equ* 263(10):6537–6575
- Shi Q-Y, Shi J-P, Song Y-L (2019a) , Effect of spatial average on the spatiotemporal pattern formation of reaction-diffusion systems, Preprint
- Shi Q-Y, Shi J-P, Song Y-L (2019b) Hopf bifurcation and pattern formation in a diffusive delayed logistic model with spatial heterogeneity. *Discrete Contin Dyn Syst Ser B* 24(2):467–486
- Simonett G (1995) Center manifolds for quasilinear reaction-diffusion systems. *Differ Integral Equ* 8(4):753–796
- Staver AC, Archibald S, Levin SA (2011a) The global extent and determinants of savanna and forest as alternative biome states. *Science* 334(6053):230–232
- Staver AC, Archibald S, Levin SA (2011b) Tree cover in sub-Saharan Africa: rainfall and fire constrain forest and savanna as alternative stable states. *Ecology* 92(5):1063–1072
- Su Y, Wei J-J, Shi J-P (2009) Hopf bifurcations in a reaction-diffusion population model with delay effect. *J Differ Equ* 247(4):1156–1184
- Turing AM (1952) The chemical basis of morphogenesis. *Philos Trans R Soc Lond Ser B* 237(641):37–72
- Wang J-F, Shi J-P, Wei J-J (2011) Dynamics and pattern formation in a diffusive predator-prey system with strong Allee effect in prey. *J Differ Equ* 251(4–5):1276–1304
- Wang J-F, Wei J-J, Shi J-P (2016) Global bifurcation analysis and pattern formation in homogeneous diffusive predator-prey systems. *J Differ Equ* 260(4):3495–3523
- Xiao Z, Brunel N, Yang Z-B, Cui X-P (2016) Constrained nonlinear and mixed effects of differential equation models for dynamic cell polarity signaling. [arXiv:1605.00185](https://arxiv.org/abs/1605.00185)
- Yan A, Xu G-S, Yang Z-B (2009) Calcium participates in feedback regulation of the oscillating ROP1 Rho GTPase in pollen tubes. *Proc Natl Acad Sci U.S.A.* 106(51):22002–22007
- Yan X-P, Li W-T (2010) Stability of bifurcating periodic solutions in a delayed reaction-diffusion population model. *Nonlinearity* 23(6):1413–1431
- Yang Z-B (2008) Cell polarity signaling in arabidopsis. *Annu Rev Cell Deve Biol* 24:551–575
- Yi F-Q, Gaffney E, Seirin-Lee S (2017) The bifurcation analysis of Turing pattern formation induced by delay and diffusion in the Schnakenberg system. *Discrete Contin Dyn Syst Ser B* 22(2):647–668
- Yi F-Q, Wei J-J, Shi J-P (2009) Bifurcation and spatiotemporal patterns in a homogeneous diffusive predator-prey system. *J Differ Equ* 246(5):1944–1977
- Yi T-M, Chen S-Q, Chou C-S, Nie Q (2007) Modeling yeast cell polarization induced by pheromone gradients. *J Stat Phys* 128(1–2):193–207
- Zheng Z-Z, Chou C-S, Yi T-M, Nie Q (2011) Mathematical analysis of steady-state solutions in compartment and continuum models of cell polarization. *Math Biosci Eng* 8(4):1135–1168
- Zhou J, Shi J-P (2015) Pattern formation in a general glycolysis reaction-diffusion system. *IMA J Appl Math* 80(6):1703–1738